Universidade de Aveiro

Departamento de Engenharia Eletrónica, Telecomunicações e Informática

2017

Vasco Manuel Nunes Mendes

Técnicas de Equalização Iterativa para Arquiteturas Híbridas Sub-Conectadas na banda de ondas milimétricas

Iterative Equalization Techniques for Sub-Connected Hybrid Architectures in the millimeter waveband

Universidade de Aveiro

Departamento de Engenharia Eletrónica, Telecomunicações e Informática

2017

Vasco Manuel Nunes Mendes

Técnicas de Equalização Iterativa para Arquiteturas Híbridas Sub-Conectadas na banda de ondas milimétricas

Iterative Equalization Techniques for Sub-Connected Hybrid Architectures in the millimeter waveband

Dissertação apresentada à Universidade de Aveiro para cumprimento dos requisitos necessários à obtenção do grau de Mestre em Engenharia Eletrónica e Telecomunicações, realizada sob a orientação científica do Doutor Adão Paulo Soares da Silva (orientador), Professor Auxiliar do Departamento de Engenharia Eletrónica, Telecomunicações e Informática da Universidade de Aveiro e do Doutor Daniel Castanheira (coorientador), investigador auxiliar do Instituto de Telecomunicações de Aveiro.

o júri / the jury

presidente /president	**Professor Doutor Aníbal Manuel de Oliveira Duarte** Professor Catedrático, Universidade de Aveiro
vogais / examiners committee	**Professor Doutor Fernando José da Silva Velez** Professor Auxiliar, Dep. De Engª Electromecânica da Fac. de Engenharia da Univ. da Beira Interior (Arguente Principal)
	Professor Doutor Adão Paulo Soares da Silva Professor Auxiliar, Universidade Aveiro (Orientador)

Agradecimentos/ acknowledgements

Em primeiro lugar, agradecer aos meus pais pelo apoio e por todo o esforço que fizeram permitindo me apostar na minha formação.

Agradecer ao meu orientador, Professor Doutor Adão Silva, ao meu coorientador, Doutor Daniel Castanheira, pela ajuda, supervisão e disponibilidade.

Ao Roberto Magueta do Instituto de Telecomunicações pela ajuda durante o desenvolvimento da plataforma de simulação.

Por último, agradecer a todos os colegas e amigos que me acompanharam ao longo destes anos, pela amizade e companheirismo.

palavras-chave

Ondas milimétricas, MIMO massivo, IB-DFE, arquiteturas hibridas analógico/digitais sub-conectadas.

resumo

As comunicações na banda das ondas milimétricas e o uso massivo de antenas são duas tecnologias promissoras que, sendo combinadas permitem alcançar elevadas taxas de transmissão, na ordem dos multi Gb/s, exigidas pelos futuros sistemas sem fios da 5G. Como estes sistemas possuem um número elevado de antenas, torna-se impossível o uso de uma arquitetura totalmente digital devido às limitações de hardware. Desta forma, é necessário projetar técnicas de processamento de sinal para arquiteturas híbridas analógico-digitais.

Dentro das arquiteturas híbridas, foram propostas duas formas de lidar com a parte analógica, que são, a forma totalmente conectada e a forma sub-conectada. Embora as arquiteturas híbridas totalmente conectadas permitam interligar todas as cadeias RF a qualquer elemento de antena, estas envolvem um elevado custo devido à sua complexidade estrutural e computacional. Assim sendo, as arquiteturas híbridas sub-conectadas tornam-se mais atraentes pois são menos exigentes do ponto de vista computacional, bem como ao nível do hardware.

Nesta dissertação, é proposto um equalizador iterativo para um sistema com uma arquitetura hibrida sub-conectada, com múltiplos utilizadores e um número massivo de antenas a operar na banda das ondas milimétricas. Os terminais dos utilizadores têm baixa complexidade e utilizam pré-codificadores aleatórios analógicos puros, cada um com uma única cadeia RF. Para a estação base, projetou-se um equalizador híbrido analógico-digital de arquitectura sub-conectada, para remover a interferência multiutilizador.

O equalizador híbrido é otimizado usando a taxa média de erro de bit como métrica. Devido ao acoplamento entre as cadeias de RF no problema de otimização, o cálculo das soluções ótimas possui elevada complexidade. Para ultrapassar este problema, calculou-se a parte analógica de cada cadeia de RF do equalizador de forma sequencial, usando um dicionário construído a partir da resposta do agregado de antenas. Compara-se o equalizador iterativo híbrido para sistemas multiutilizador de arquitectura sub-conectada proposto com uma abordagem híbrida analógica/digital totalmente conectada, recentemente proposta na literatura e com uma arquitetura totalmente digital. Os resultados mostram que o desempenho do esquema proposto aproximasse da abordagem híbrida totalmente conectada após apenas algumas iterações.

keywords

Millimeter-wave, massive MIMO, IB-DFE, sub-connected hybrid analog/digital architectures.

abstract

The millimeter wave communications and the use of a massive number of antennas are two promising technologies that being combined allow to achieve the multi Gb/s required by future 5G wireless systems. As this type of systems has a high number of antennas it is impossible to use a fully digital architecture, due to hardware limitations. Therefore, the design of signal processing techniques for hybrid analog-digital architectures is a requirement.

Depending on the structure of the analog part the hybrid analog-digital architectures may be fully connected or sub-connected. Although the fully connected hybrid architectures allow to connect all RF chains to any antenna element, they involve a high cost due to its structural and computational complexity. As such, the sub-connected hybrid architectures become more attractive, since either at the hardware level or from the computational point of view they are less demanding.

In this dissertation, we propose a hybrid iterative block multiuser equalizer for sub-connected millimeter wave massive MIMO systems. The user terminal transceiver has low-complexity and as such employ a pure analog random precoder, with a single RF chain. For the base station, a sub-connected hybrid analog-digital equalizer is designed to remove the multiuser interference.

The hybrid equalizer is optimized using the average bit-error-rate as a metric. Due to the coupling between the RF chains in the optimization problem the computation of the optimal solution is way too complex. To address this problem, we compute the analog part of the equalizer sequentially over the RF chains using a dictionary built from the array response vectors. The proposed sub-connected hybrid iterative multiuser equalizer is compared with a recently proposed fully connected hybrid analog-digital approach and with the fully digital architecture. The results show that the performance of the proposed scheme is close to the fully connected hybrid approach after just a few iterations.

Contents

List of Figures

List of Tables

List of Abbreviations

1G	1st Generation
2G	2nd Generation
3D	Three-Dimensional
3G	3rd Generation
4G	4th Generation
5G	5th Generation
AA	Array Antenna
BER	Bit Error Rate
BF	Beamformer
BS	Base Station
CSI	Channel State Information
DFE	Decision Feedback Equalizer
DFT	Discrete Fourier Transform
EGC	Equal Gain Combining
FDM	Frequency-Division Multiplexing
FDMA	Frequency-Division Multiple Access
GSA	Global mobile Suppliers Association
GSM	Global System for Mobile Communications
HPB	Half Power Beam
HPBW	Half Power Beam Width
IB-DFE	Iterative Block Decision feedback equalizer
IDFT	Inverse of Discrete Fourier Transform
ISI	Intersymbol Interference
LTE	Long Term Evolution
LTE-A	LTE-Advanced
MIMO	Multiple-Input-Multiple-Output

MISO	Multiple-Input-Single-Output
mMIMO	Massive MIMO
MMSE	Minimum Mean Squared Error
mmWave	Millimeter Wave
MRC	Maximal Ratio Combining
MSE	Mean Squared Error
OFDM	Orthogonal Frequency-Division Multiplexing
PA	Power Amplifier
PLP	Physical Layer Pipes
PS	Phase Shifter
QoS	Quality of Service
QPSK	Quadrature Phase-Shift Keying
RF chain	Radio Frequency Chain
SC	Selection Combining
SFBC	Space Frequency Block Code
SIMO	Single-Input-Multiple-Output
SINR	Signal-to-Interference-plus-Noise Ratio
SISO	Single-Input-Single-Output
SNR	Signal-to-Noise Ratio
STBC	Space Time Block Code
TDD	Time Division Duplex
TDMA	Time-Division Multiple Access
TFS	Time-Frequency Slicing
TI	Time Interleaving
UCA	Uniform Circular Array
ULA	Uniform Linear Array
UPA	Uniform Planar Array
URA	Uniform Rectangular Array
UT	User Terminal

UTRA	Universal Terrestrial Radio Access
V-BLAST	Vertical Bell Labs Layered Space-Time
WCDMA	Wide-Band Code-Division Multiple Access
WLAN	Wireless Local Area Networks
WRC	World Radiocommunications Conferences
ZF	Zero Forcing

1 Introduction

This dissertation begins with an introduction to the evolution of mobile communication systems, culminating in the next 5th Generation (5G) of wireless systems. In fact, the future 5G systems are the global theme that motivated the research work addressed in this document. In this chapter, the evolution path of the mobile communication systems is discussed from the beginning until the today systems. Some key requirements to achieve the desired quality of service (QoS) are presented, as well as the main objectives for the future 5G. Then the motivations, objectives and the main contributions are presented.

1.1 Mobile Communication Evolution

The demand for more efficient services to meet the people needs has led to a constant evolution of telecommunications. The first generation of mobile telecommunication technologies, commonly denominated as the first generation (1G), offered basic voice services supported by analog transmission. The second generation (2G) systems apart from the voice services, already supported in the 1st generation, also included low rate data services. The major difference between the 1G and the 2G was the upgrade from analog to digital transmission technologies. Among the most important 2G systems, we have Global System for Mobile Communications (GSM) which is based on the combination of Time-Division Multiple Access (TDMA) and Frequency-Division Multiple Access (FDMA). After 2G, new services were enabled to support new necessities of the humankind. The third Generation Partnership Project (3GPP) emerged in 1998 with the purpose to produce technical specifications and technical reports for a 3rd Generation (3G) mobile system. This 3G mobile system was based on evolved GSM core networks and the radio access technologies that they support, i.e., Universal Terrestrial Radio Access (UTRA) both Frequency Division Duplex (FDD) and Time Division Duplex (TDD) modes [1]. The

underlying 3G of the mobile communications enable mobile broadband services, faster and better connections and has improved the security with Wide-Band Code-Division Multiple Access (WCDMA) [2],[3]. The fourth generation (4G) show up with an orthogonal frequency-division multiplexing (OFDM)-based radio access technology eliminating the bandwidth problems evidenced in 3G technology and jointly with the Multiple-Input-Multiple-Output (MIMO) concept to achieve better and more efficient transmissions [3]. With capacity for high speed data, significant spectral efficiencies and adoption of advanced radio techniques, the emergence of 4G has been the basis for all new mobile systems. The Long Term Evolution (LTE) is a 4G radio access technology, based on OFDM, which supports a scalable transmission bandwidth up to $20\ \text{MHz}$ and advanced multi-antenna transmission [3]. Nowadays, LTE-Advanced (LTE-A) is the most efficient mobile broadband technology commercially available Today the best mobile technology available [3]. This development must continue and new technologies must be developed, as well as systems capable of offering more and better services.

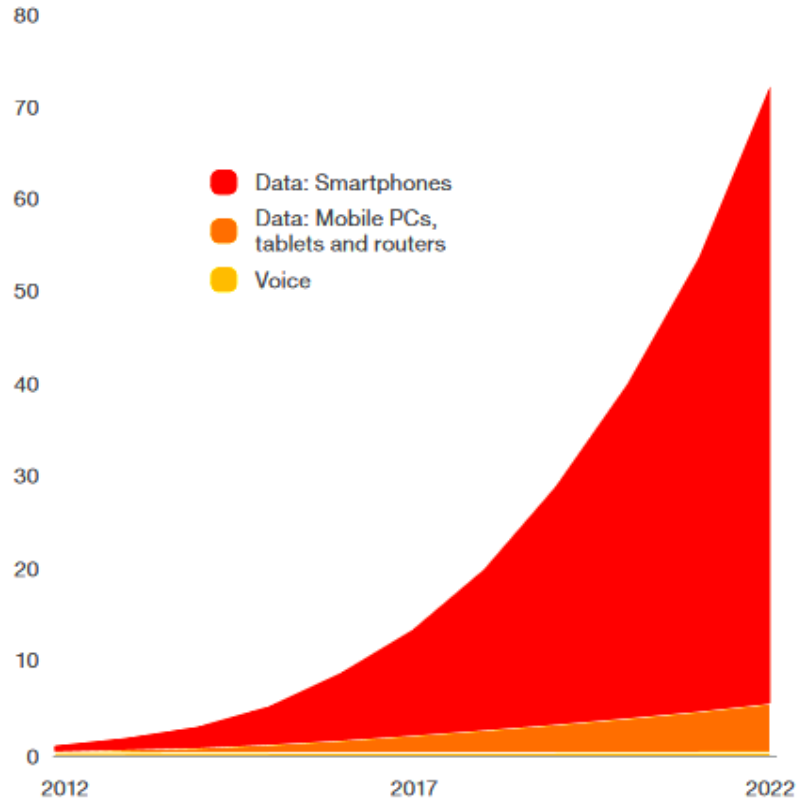

Fig. 1: Global mobile traffic (ExaBytes per month) [4].

As shown in Fig. 1, according to a study conducted by Ericsson in [4], monthly smartphone data traffic continues to increase in all regions of the world, despite the large differences in data consumption patterns between networks, markets and subscribers. According to this study, it is thought that more than 90% of mobile data traffic will come from smartphones in 2022.

As suggested in [5], User Experience, Connectivity, Intelligence, Reliability and Efficiency are five great values for the new mobile generation. For now, it is sensible to state that the true evolution to the new mobile generation will be achieved through the evolution of the existing systems LTE/LTE-A and also through a completely new technological revolution [5].

1.2 The Next Mobile Generation

As the radio interface of mobile phones has evolved, it has typically been changed about every ten years, and the 5G interface is expected to start being used in the 2020s. Thus, the new mobile generation will be an evolution of 4G systems. Fig. 2 shows the inter-relationship between LTE-Advanced development and new 5G research and development areas. It is possible to observe that a true evolution to 5G can be achieved by pursuing both, continued technological evolution builds upon the existing LTE/LTE-A and a completely new revolution of technology, providing more data to more people and converging a lot of new applications.

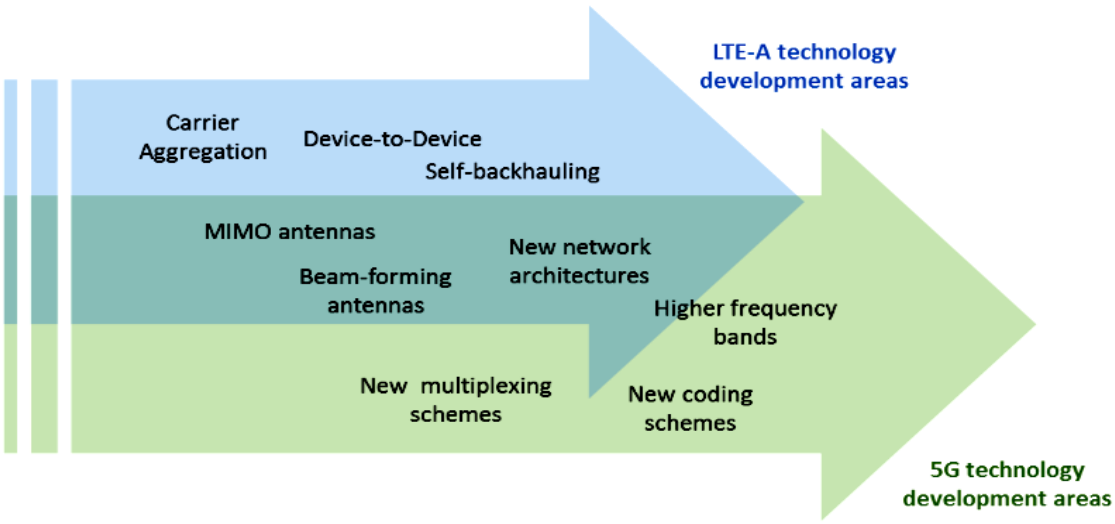

Fig. 2: Some research and development areas for future wireless networks [6].

Currently the mobile applications are very diverse and present different requirements for the network, in particular, in terms of latency, peak data throughput, connection density, throughput density and device power. To maximize its potential, 5G networks will need to meet the varied requirements, and support allocation of resources to different applications in an intelligent way. Based on discussions with vendors and a review of current discussions on the topic, in [6] the Global mobile Suppliers Association (GSA) considers the values in the table below to be sensible minimum parameters that will define 5G.

Tab. 1: Functional performance criteria for 5G [6].

Parameter	Value
Latency in the air link	< 1 ms
Latency end-to-end (device to core)	< 10 ms
Connection density	$100\times$ compared with LTE
Area capacity density	1 Tbit/s/Km^2
System spectral efficiency	10 bit/s/Hz/cel
Peak throughput (downlink) per connection	10 Gbit/s
Energy efficiency	$> 90\%$ improvement over LTE

With regard to the systems of the 5G, the field of research presents some key technologies like millimeter wave communications (mmWave) and massive MIMO (mMIMO) [7],[8]. While mmWave allows higher frequency bandwidths than currently used, mMIMO can scale up the conventional MIMO by orders of magnitude [9]. Several researches have been carried out in order to utilize these technologies on the future systems and to achieve the requirements of the 5G mobile technology, as in [10] and [11].

1.3 Motivation and Objectives

The constant mobile systems evolution has enabled an exponential grow of the number of mobile devices distributed around the world, as well as an increase of the available services. With this constant evolution, the necessities of the humankind also increase. The research field works in this direction trying to develop technology able to offer better performance and QoS. As mentioned above, mmWave and mMIMO are considered as two key enabling technologies to achieve the QoS requirements of future 5G systems.

One of the most important advantages of mmWave communications is that the frequency resource is abundant and the size of the antennas can be considerably reduced.

Thus, there is already research ongoing to explore the large bandwidth in the mmWave band to reach very high transmission rates. The first IEEE wireless standard for data rates over 1 Gb/s was the 802.15.3c, using 57−66 GHz band (mmWave) [12]. As addressed in [12] the 802.15.3c allows to achieve 3.8 Gbit/s for video streaming and multivideo streaming. Recently, the 802.11ad protocol which enables multigigabit speed levels (up to 7 Gbit/s) on Wireless Local Area Networks (WLANs), using signal transmission at 60 GHz [13]. Although the clear advantages, these protocols are mmWave based they have been standardized for short range services and indoor communication.

The use of multiple antennas has been also an active area of research because the MIMO concept has become quite attractive to increase the capacity and reliability of wireless communications systems. The concept of massive MIMO systems has come up with the idea of utilizing the advantages of large array antenna elements in terms of huge capacity gains, bigger than the present MIMO systems, which are using either two or four antennas [14]. Furthermore, the large antenna gain and the enhanced spatial processing resulting from mMIMO, can compensate the propagation difficulties of mmWave communications [8] and due to the lower wavelength the mmWave band is more suitable to pack a large number of antennas at the transceivers in a small form factor.

The combined use of mmWave with mMIMO is very promising because systems with these two technologies can efficiently exploit spatial processing techniques such as beamforming/precoding and spatial multiplexing on the transmitter and/or receiver sides [15]. With the high number of antennas used in these systems it is not practical to have a fully-dedicated radio frequency (RF) chain for each antenna as in conventional MIMO systems. The reason for that is the high power consumption and the high cost of mmWave mixed-signal components. On the other hand, analog beamforming is a simple and effective method to realize the beamforming gains from a large number of antennas but less flexible than digital beamforming and usually used in single user based scenarios [15]. Thus, it is necessary to achieve a trade off between both analog and digital technologies.

The hybrid analog/digital architecture where some signal processing (transmit and receive beamforming) is done at the digital level and some left to the analog domain, is considered as a solution to alleviate the hardware constraints of the mmWave mMIMO systems. Along these research lines some proposals have been recently discussed presenting

hybrid analog/digital beamforming for mmWave mMIMO [16]-[18]. Specifically, for multiuser systems, some beamforming approaches have been proposed for fully connected hybrid architectures [19]-[21], where each RF chain is connected to all antennas. In alternative to the fully connected architecture, we have also the sub-connected architecture that allow us to reduce the number of used phase shifters (PSs) since each RF chain can only be connected to a subset of antennas [22]. The fully connected hybrid architectures for mmWave mMIMO have higher computational cost as well as power consumption, which is used to excite and to compensate the insertion loss of PSs [22]. In counterpart, the recent research works demonstrate that the fully connected architectures achieve better BER performances than sub-connected architectures.

As mmWave and mMIMO are a promising combination to achieve the multi Gb/s required by future 5G wireless systems and the fully digital architectures are not feasible due to their complexity and hardware limitations, there is a need to design signal processing techniques for hybrid analog-digital architectures, especially for the sub-connected architecture. Therefore, the aim of this work is to implement an efficient hybrid iterative multiuser equalizer for a sub-connected hybrid architecture for mmWave mMIMO systems. The hybrid analog-digital multiuser equalizer approach proposed in [21] for full connected architecture is extended for a sub-connected one. The limitation that each RF chain is only physically connected to a sub-set of antennas makes the design of the proposed sub-connected hybrid iterative multiuser equalizer harder than for the fully connected based approaches. The proposed sub-connected hybrid iterative multiuser equalizer is compared with a recently proposed fully connected approach. The results show that the performance of the proposed scheme is close to the fully connected hybrid approach counterpart after just a few iterations.

1.4 Contributions

The main contribution of this dissertation was the development of an iterative multiuser equalization scheme for sub-connected hybrid mmWave mMIMO architectures, which originated the following article:

R. Magueta, V. Mendes, D. Castanheira, A. Silva, R. Dinis and Atilio Gameiro, "Iterative Multiuser Equalization for Sub-Connected Hybrid mmWave Massive

MIMO Architecture", submitted to Wireless Communications and Mobile Computing Journal.

1.5 Outline of the Dissertation

From this point onward, the dissertation structure is organized in the following form:

Chapter 2 presents the main multiple antenna techniques and what advantages these techniques bring in terms of diversity, spatial multiplexing and beamforming. The massive MIMO concept, which is a key enabling technology for 5G, is also, introduced in this chapter.

Chapter 3 first introduce the single carrier and multicarrier concepts. Digital techniques of equalization, as linear and non-linear based equalizers, are very important to understand the developed work. Thus, two algorithms for linear structures and an iterative structure, which is performed on a per-block basis, are also discussed in this chapter.

The millimeter wave technology is introduced in chapter 4, where we present the spectrum bands, the propagation characteristics, as well as the channel model that is considered in the remainder of this dissertation. It is also in this fourth chapter that we present one of the most important concepts of the dissertation, the sub-connected hybrid analog/digital architectures for mmWave mMIMO systems, with special focus put on the analog part.

The aim of the second, third and fourth chapters is to present the essential background for the main subject addressed in the implementation part of this work, that is the evaluation of the performance of the proposed algorithms for the sub-connected hybrid architecture for mmWave mMIMO systems, presented in the next chapter.

All system characterization and algorithm design are described in chapter 5, as well as its performance. Results about the BER performance are also presented to evaluate the proposed algorithms and implementation against two other algorithms from the literature.

Finally, in chapter 6 the conclusions of this work and some guidelines for the future research are presented.

1.6 Notations

Matrices are denoted in boldface capital letters and column vectors in boldface lowercase letters. The operations $tr(.)$, $(.)^*$, $(.)^H$, $(.)^T$ and $(.)^H$ represent the trace, the conjugate, the transpose, and the Hermitian transpose of a matrix. The operator $\text{sign}(a)$ represents the sign of real number a and $\text{sign}(c) = \text{sign}(\Re(c)) + j\,\text{sign}(\Im(c))$ if c is a complex number. It can also be employed element-wise to matrices. The functions $\Re(c)$ and $\Im(c)$ represent the real part and imaginary part of c, respectively. The functions $\text{diag}(\mathbf{a})$ and $\text{diag}(\mathbf{A})$, where $\mathbf{a}$ is a vector and $\mathbf{A}$ a square matrix, correspond to a diagonal matrix where the entries of the diagonal are equal to $\mathbf{a}$, and to a vector equal to the diagonal entries of $\mathbf{A}$, respectively. The element of row j and column l of the matrix $\mathbf{B}$ is denoted by $\mathbf{B}(j,l)$. The identity matrix $N \times N$ is $\mathbf{I}_N$.

2 Wireless Systems with Multiple Antennas

Multiple antennas are an important means to improve the performance of wireless systems. There are three types of fundamental gains, obtained through multiple antennas systems, that we address in this chapter: multiplexing gain, diversity gain, and antenna gain. Furthermore, with this type of systems, it is possible to explore spatial properties of the radio channels to improve the QoS. This chapter presents the different multiple antenna techniques as well as the advantages that these mechanisms bring through diversity, spatial multiplexing and beamforming. The use of multiple antennas has enabled a significant improvement in mobile communications. However, current systems do not experience all of these benefits because they use a small number of antennas. In this chapter the concept of massive MIMO is also introduced, since it is seen as a key enabling technology for future 5G systems.

2.1 Diversity

The fading effect can be mitigated by transmitting the same signal through different fading channels. By doing that the probability that all replicas of the signal will fade simultaneously is reduced. This approach defines the diversity concept that is commonly used to overcome degradation in performance due to interference and fading. Wireless mobile systems constantly resort to diversity techniques with the aim to reduce the multipath fading effects. Furthermore, these techniques can allow to improve the reliability of transmission. In a system, diversity order is represented by the number of the diversity channels [23]. Diversity can be achieved using the time, frequency and space domains. The utilization of time/frequency diversity incurs an expense time in the case of time diversity and bandwidth in the case of frequency diversity to introduce redundancy. The use of multiple antenna systems allows the introduction of a new way to achieve diversity which is the space domain. This technique requires a simple transmit antenna but multiple receive antennas. By transmitting the same signal to different receive antennas it is expected that the

different received signals will experience different fading effects, permitting a constructive combining of the different signals, improving the error performance.

2.1.1 Time Diversity

Time diversity implies interleaving and coding over symbols across different coherent time periods. This technique permits to mitigate channel fading at a cost of additional time delay and loss of bandwidth efficiency [23]. As shown in Fig. 3 the main idea of time interleaving (TI) is to interlace multiple codewords so that each codeword is transmitted over an extended period of time. In this example, four codewords are interleaved in succession, however another interleaving method could be used. If there is destructive interference of multipath originating a fading of the channel during a coherent time period, the receiver can lose important information. Fig. 3 shows the two cases in which one interleaving is used and the other not. When interleaving is implemented it is possible to retrieve information even in the case of deep channel fading, due to the fact that every part of the codeword is affected by different fading along the time. Thus, only part of the codeword will being missing not all the codeword.

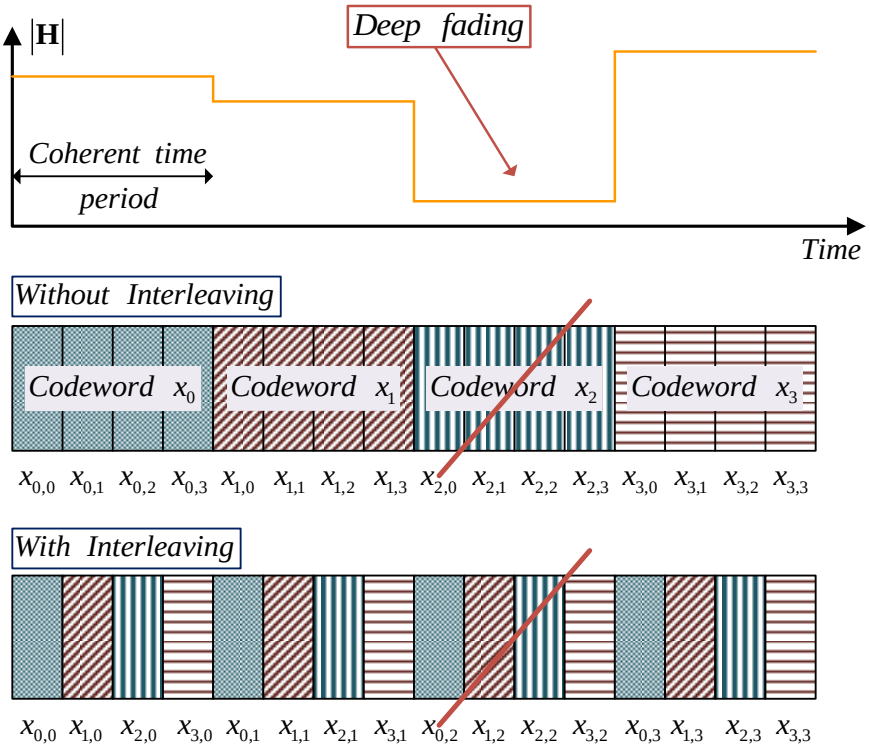

Fig. 3:Time diversity using interleaving.

The total period of time over which one codeword is transmitted is referred to as interleaving duration. Thus, the implementation of TI implies an increase in the hardware complexity of the receivers, because it is necessary enough memory to store all the codewords that were interleaved at the transmitter, as well as an increase of the end-to-end latency. Furthermore, the maximum interleaving duration that can be provided for any given data rate is constrained by the time deinterleaving memory, which is available in the receiver [24].

Another technique which is based on the time diversity principle is the TDMA, where the transmission is divided into time slots and only one user is allowed to either transmit or receive in each time slots. With this technique, a channel might be a particular time slot that reoccurs at slot locations in every frame. Thus, TDMA shares a single carrier frequency among many users, where each user uses a non-overlapping time slot. Mobile broadcasting systems generally employ discontinuous transmissions in order to reduce the power consumption of the receivers. However, the maximum time diversity is achieved when no time slicing is used (i.e. maximum power consumption) and the codewords are continuously transmitted over time.

2.1.2 Frequency Diversity

To achieve frequency diversity, the same information can be transmitted using different frequencies, i.e., the interleaving in the frequency domain or frequency hopping. Frequency hopping, used in GSM and other technologies also, is based on this diversity concept. Due to the fact that frequency interleaving (FI) is performed in the frequency domain, it has no constraints in terms of latency or channel switching time [24]. The FDMA technique assigns a single RF channel, or frequency band, to a single user. Thus, is allocated a single frequency band with 25-30 kHz, which supports only one user per carrier [23]. These bands are assigned on demand to users who request for service. No other users can share the same frequency band during a call made. If an FDMA channel is not in use it sits idle and cannot be used by other users to increase the system capacity. Furthermore, it cannot be used by other users even if a user stays in pause during a phone call.

While the signal bandwidth is generally limited to one RF channel, it may be possible to extend the frequency interleaving across multiple channels by means of time-frequency slicing [24]. As shown in Fig. 4 Time-Frequency Slicing (TFS) employs a combination of

frequency hopping and time slicing. This technique implies a virtual bundling of multiple RF channels that do not necessarily have to be adjacent to each other, which increases the frequency diversity of the system significantly and therefore offers enhanced robustness [25]. In the TFS example presented in the Fig. 4 the total capacity of the system is divided into a several Physical Layer Pipes (PLPs), where the data of a specific service are sent. The data in each PLP is then interleaved independently of all other PLPs and is equally fragmented and transmitted over all bundled channels. Furthermore, the data of one PLP is never transmitted simultaneously on multiple channels, but on a single channel only. Thus, if one RF channel is strongly attenuated or disturbed by an interferer, the receiver may still be able to compensate this weak channel by listen the other channels and combine the information. However, this also leads to a significantly increased complexity within the receiver.

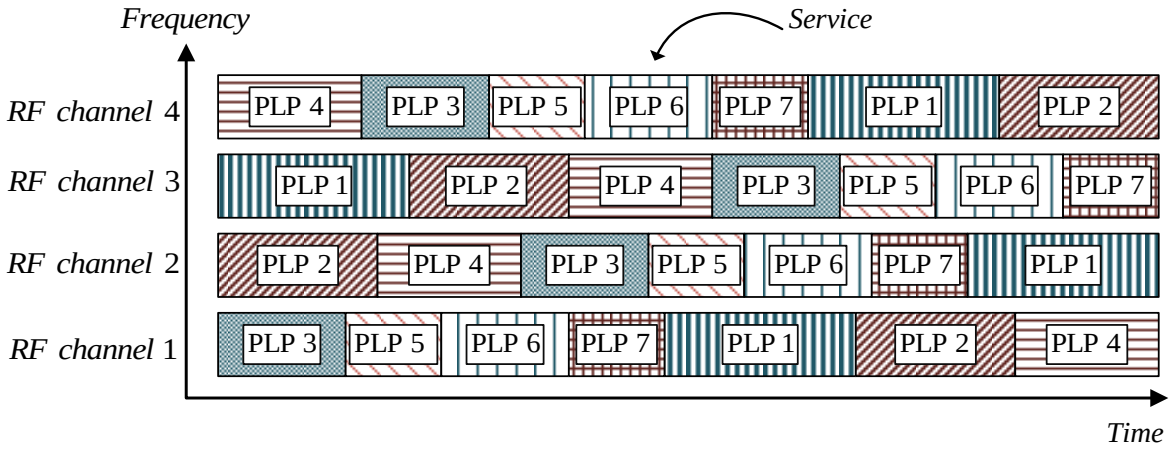

Fig. 4:Time-frequency slicing.

The OFDM technique, used for 4G systems, is based on the technique of Frequency-Division Multiplexing (FDM). In FDM different streams of information are mapped onto separate parallel frequency channels. Each FDM channel is separated from the others by a frequency guard band to reduce interference between adjacent channels. These methods imply assignment of different frequency bands, which can represent a limitation, because the current available frequency band is a limited resource.

2.1.3 Spatial Diversity

Spatial diversity is different than time and frequency diversity because unlike those, spatial diversity needs no additional power and bandwidth at the transmission. The

possibility to set multiple antennas sending the same information through independent paths and combining them to mitigate fading effects is the principal aim of spatial diversity. In a multiple antenna system the number of diversity paths is given by $N_{rx}N_{tx}$, where N_{rx} is the number of receive antennas and N_{tx} is the number of transmit antennas. Thus, redundancy is achieved from replicas of the transmitted signal sent and received by multiple independent antennas.

Fig. 5 shows the three configurations in multiple antenna systems. In Fig. 5-a) is presented the multiple-input-single-output (MISO) case, in Fig. 5-b) the single-input-multiple-output (SIMO) case and in Fig. 5-c) the multiple-input-multiple-output (MIMO) case. Contrary to the MISO (SIMO) architectures where we can only explore the transmit (receive) diversity in the MIMO architecture we may combine the transmit and receive diversities.

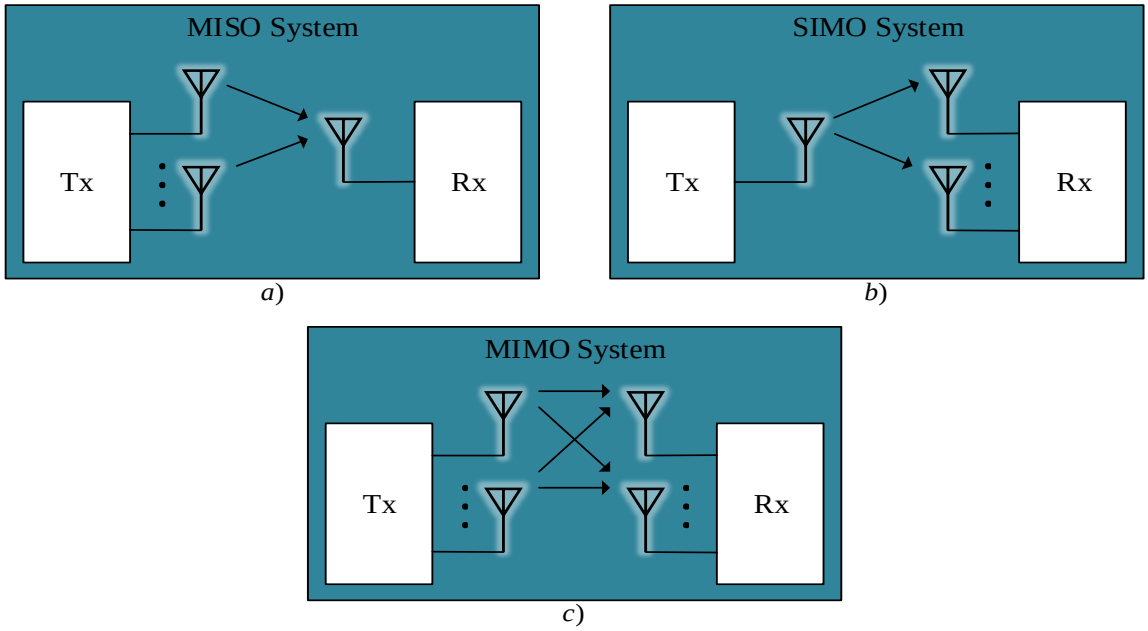

Fig. 5: Different multiple antenna systems configurations; a) MISO system; b) SIMO system; c) MIMO system.

2.1.4 Receive Diversity

Since it is easier and more cost effective to use multiple antennas at the Base Station (BS) than in the UT, this technique is mostly associated to the uplink communication. Multiple antennas are use at the receiver to obtain diversity and employ switching and combining or selection intending to improve the quality of received signal. As it can be seen

in the Fig. 6 N_{rx} represents de number of receiver antennas and the received signal will be given by

$$\begin{bmatrix} y_1 \\ \vdots \\ y_{N_{rx}} \end{bmatrix} = \begin{bmatrix} h_1 \\ \vdots \\ h_{N_{rx}} \end{bmatrix} x + \begin{bmatrix} n_1 \\ \vdots \\ n_{N_{rx}} \end{bmatrix}. \tag{1}$$

Thus, the transmitted signal with the respective data symbol x, the channel matrix $\mathbf{H} \in \mathbb{C}^{N_{rx}}$ and the noise matrix $\mathbf{n} \in \mathbb{C}^{N_{rx}}$ are used to find or build the received signal $\mathbf{y} \in \mathbb{C}^{N_{rx}}$. With the estimated symbols obtained through the equalizer vector $\mathbf{g} \in \mathbb{C}^{N_{rx}}$ and given by

$$\hat{\mathbf{s}} = \begin{bmatrix} g_1 & \cdots & g_{N_{rx}} \end{bmatrix} \begin{bmatrix} y_1 \\ \vdots \\ y_{N_{rx}} \end{bmatrix} = \begin{bmatrix} g_1 & \cdots & g_{N_{rx}} \end{bmatrix} \begin{bmatrix} h_1 \\ \vdots \\ h_{N_{rx}} \end{bmatrix} \mathbf{x} + \begin{bmatrix} g_1 & \cdots & g_{N_{rx}} \end{bmatrix} \begin{bmatrix} n_1 \\ \vdots \\ n_{N_{rx}} \end{bmatrix}. \tag{2}$$

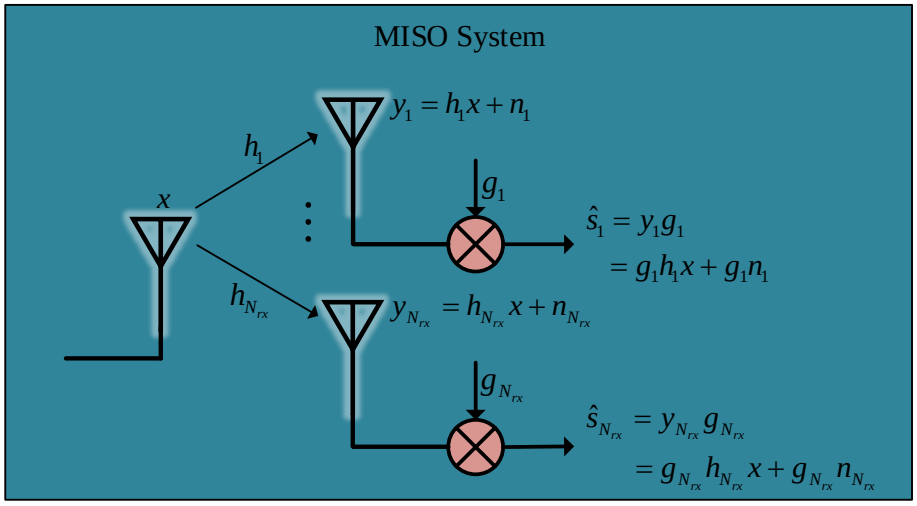

Fig. 6: MISO system.

To combine the multiple received signals there are some diversity combining methods, which are organized from the best to the worst in the following list [26]:

1. **Maximal Ratio Combining (MRC):** Also known as Matched Filter, in this algorithm each received signal is individually co-phased and weighted on their signal to noise ratio (SNR) before summing;
2. **Equal Gain Combining (EGC):** For this algorithm, the signals are co-phased on each branch and then summed;

3. **Selection Combining (SC):** This is an algorithm of selection which compares the instantaneous amplitude of each channel and chooses the antenna branch with the highest amplitude, ignoring the other signal antennas;
4. **Switched Combining:** Uses only one antenna at a time because in this method the system switches to the next antenna only when the current received signal falls below a certain value.

As the Maximal Ratio Combining (MRC) and the Equal Gain Combining (EGC) are the algorithms with the best performance-complexity trade-off from the previous list, they will be presented in more detail in the following.

1. Maximal Ratio Combining

The MRC technique is a linear combining method based on the SNR presented by each antenna branch. The MRC based combiner compensates the phases and weights of each signal according to their SNR in order to maximize it and eliminate bad channel conditions. For the MRC technique, the optimal weights in fading is

$$g_m = h_m^*, \tag{3}$$

where $m \in \{1,...,N_{rx}\}$ and the diversity achievable at the output combiner is

$$\hat{\mathbf{s}}_{MRC} = \sum_{m=1}^{N_{rx}} |h_m|^2 x + \sum_{m=1}^{N_{rx}} h_m{}^* n_m \tag{4}$$

Assuming i.i.d Rayleigh fading on each branch, this method permits to achieve an antenna gain, A_g, that will be equal to the number of receive antennas. The antenna gain increases linearly with the number of branches.

For the uplink, MRC is the most promising single-user detection technique since the spreading codes do not superpose in an orthogonal fashion at the receiver and maximization of the signal-to-interference ratio is optimized [27].

2. Equal Gain Combining

For the EGC technique, the branch weights are all set to be equal, therefore, it does not require the knowledge of channel amplitudes. However, the signals from each branch area co-phased to provide equal gain combining. Thus, the receiver can exploit signals that are simultaneously received on each branch. These weights are given by

$$g_m = \frac{h_m^*}{|h_m|}, \tag{5}$$

where $m \in \{1,...,N_{rx}\}$. Using these weights, the signal at the output combiner is

$$\hat{\mathbf{s}}_{EGC} = \sum_{m=1}^{N_{rx}} |h_m| x + \sum_{m=1}^{N_{rx}} \frac{h_m^*}{|h_m|} n_m . \tag{6}$$

In this case the, achievable antenna gain is given by

$$A_g = \left(1 + \frac{\pi}{4}(N_{rx} - 1)\right), \tag{7}$$

considering i.i.d Rayleigh fading on each branch. Also for this technique, the antenna gains increase linearly with the number of branches, however less than MRC.

As demonstrated in [28], although the EGC is less complex the performance of MRC is slightly better. Both methods achieve the same diversity, however, the EGC method provide lower antenna gains.

2.1.5 Transmit Diversity and Space-Time Coding

Unlike receive diversity, transmit diversity needs multiple transmitting antennas, as shown in Fig. 7. This signal processing technique should be used to extract the noisy and distorted received signal in transmit diversity. To achieve diversity there are two main classes: close-loop transmit diversity and open-loop transmit diversity.

1. Close-loop transmit diversity

In the closed loop case, two or more copies of the signal are sent by the transmitter, applying a phase shift to one or more signals before the transmission. Thus, the risk of destructive interference can be avoided because the signals are send in phase. The Channel State Information (CSI) is available at the transmitter in the closed loop case. Therefore, the receiver assists in channel estimation and feedback of these estimates to the transmitter. In this case, a reduced-complexity estimation and feedback process at the receiver along with

simple processing at the transmitter will reduce consumption of system resources and result in an efficient communication system [29].

2. Open-loop transmit diversity

For the open loop case, we have some advantages like the possibility of not requiring the CSI knowledge or robustness against adverse conditions, however the performance is usually lower than closed loop approaches. To get transmit diversity, without the CSI available, there are some important techniques that can be used. The approach to space-time and space-frequency coding based on encoding blocks of data, called Space-Time Block Code and Space-Frequency Block Code (STBC/SFBC), allows to increase diversity. In this approach, the symbols are arranged in a such a way that, at the receiver, maximum-likelihood decoding can be performed individually on each symbol independent of the other symbols. The data symbols, effectively, are 'orthogonal' to each other. For example, with a system with two antennas at the transmitter it can be used the STBC technique called Alamouti coding [30]. The Alamouti coding aim to give orthogonal feature to data stream, which bring symbol separation at the receiver.

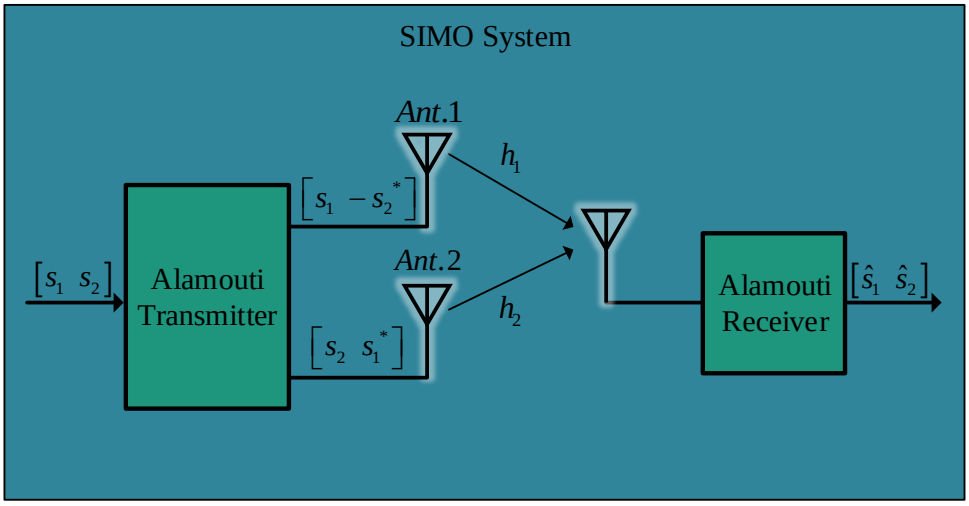

Fig. 7: Alamouti scheme applied in a SIMO system (2x1).

As shown previously in the Fig. 7 the matrix with the transmitted symbols is given by

$$\mathbf{s} = \begin{bmatrix} s_1 & -s_2^* \\ s_2 & s_1^* \end{bmatrix}, \tag{8}$$

where the transmitted symbols at the first instant are s_1 and s_2, respectively by Ant.1 and Ant. 2, therefore, at the second instant are $-s_2^*$ and s_1^*, again by Ant. 1 and Ant. 2. By (8) we can see that

$$s_1 s_2 - s_2^* s_1^* = 0\,, \tag{9}$$

which means that those codes are orthogonal. Assuming again the example of the Fig. 7, the received signal at time/frequency is given by

$$\begin{cases} y_1 = \frac{1}{\sqrt{2}} h_1 s_1 + \frac{1}{\sqrt{2}} h_2 s_2 + n_1 \\ y_2 = -\frac{1}{\sqrt{2}} h_1 s_2^* + \frac{1}{\sqrt{2}} h_2 s_1^* + n_2 \end{cases}, \tag{10}$$

where y_1 and y_2 is the received signal at the first instant and at the second instant respectively and $1/\sqrt{2}$ represents the power constraint in order to normalize the power per symbol to one. At the Alamouti decoder, the estimated symbols, in both instants, are obtained by

$$\begin{cases} \hat{s}_1 = \frac{1}{\sqrt{2}} h_1^* y_1 + \frac{1}{\sqrt{2}} h_2 y_2^* + n_1 \\ \hat{s}_2 = -\frac{1}{\sqrt{2}} h_2 y_1^* + \frac{1}{\sqrt{2}} h_1 y_2^* + n_2 \end{cases} \tag{11}$$

Thus, assuming that h_n is equal for both instants, where $n \in \{1,..., N_{tx}\}$ and $N_{tx} = 2$, the soft decision of data symbol s_1 is given by

$$\hat{s}_1 = \frac{1}{2}\left(h_1^* h_1 + h_2 h_2^*\right) s_1 + \frac{1}{\sqrt{2}} h_1 n_1 + \frac{1}{\sqrt{2}} h_2 n_2^*\,. \tag{12}$$

The interference caused by data symbol 2 is fully eliminated because the channels between two adjacent instants or frequencies are highly correlated. As can be seen in [28] the SNR is given by 3dB losses compared to the MRC. This simplest coding scheme, where the bandwidth is not expanded, allows to apply orthogonal codes only for 2 transmit antennas $\left(N_{tx} = 2\right)$ and for N_{rx} receiver antennas [28]. Therefore, this scheme can be used not only for MISO systems but also for MIMO systems. For more than two transmit antennas, there are the Tarokh orthogonal codes or the Quasi-Orthogonal codes [31],[32]. The Tarokh codes have the disadvantage of having a code rate less than 1, thus it is required an expansion of

the bandwidth. The Quasi-Orthogonal codes were proposed to overcome this code rate and required bandwidth expansion problem, however, they cannot obtain full diversity.

2.2 Spatial Multiplexing

The MIMO technology was an important advance for current 4G cellular systems and it is expected as a key technology for future 5G systems, jointly with other innovative technologies. As represented in Fig. 8, MIMO systems use multiple antennas at the transmitter and receiver side, where N_{rx} and N_{tx} represents the number of receiver and transmitter antennas, respectively. A MIMO received signal can be built through a simple translation of the Fig. 8 into a mathematical expression or into a matrix/vector expression, as follows:

$$\mathbf{y} = \mathbf{H}\mathbf{x} + \mathbf{n}, \tag{13}$$

where the transmitted signal $\mathbf{x} \in \mathbb{C}^{N_{tx}}$, the channel $\mathbf{H} \in \mathbb{C}^{N_{rx} \times N_{tx}}$ and the noise $\mathbf{n} \in \mathbb{C}^{N_{rx}}$ are used to find or build the received signal $\mathbf{y} \in \mathbb{C}^{N_{rx}}$. MIMO systems have brought the spatial multiplexing idea that was firstly published in [33], where the major application was high definition television field. In contrast to spatial diversity techniques, where the main objective is to improve the error performance, spatial multiplexing aims to provide higher bit rates compared to a single-antenna system.

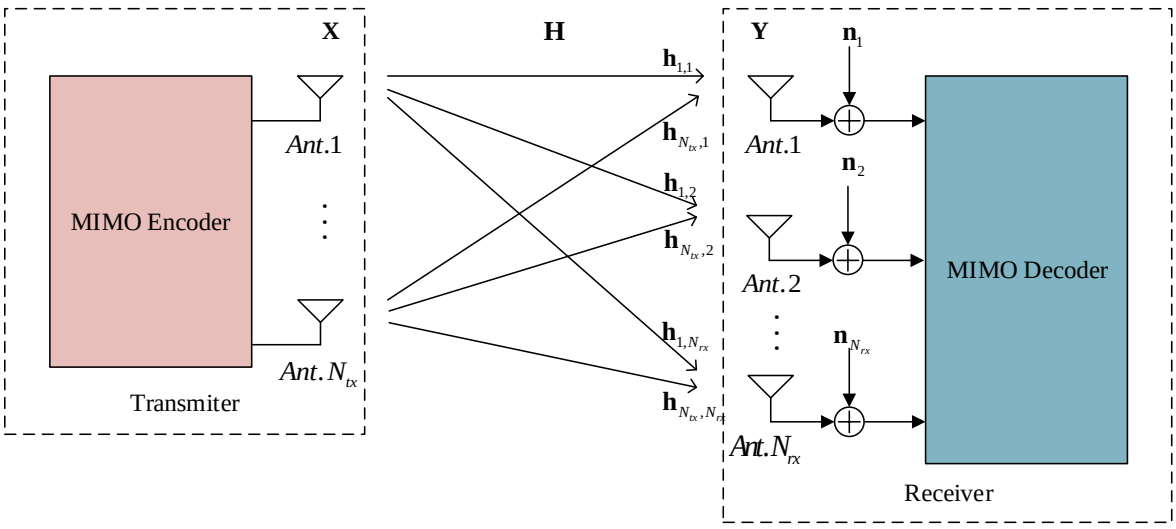

Fig. 8: Generic representation of a MIMO System.

The capacity of a MIMO system with N_{tx} transmit and N_{rx} receive antennas grows (approximately) linearly with $\min\{N_{tx}, N_{rx}\}$, without requiring extra bandwidth or extra transmission power [34]. However, if the number of transmit antennas exceeds the number of receive antennas the system becomes inherently rank-deficient [34]. Thus, it is necessary to respect the condition $N_{rx} \geq N_{tx}$ for a system with spatial diversity gain accomplished, allowing to provide higher bit rates. Several different data bits transmitted across several independent (spatial) channels allow for higher bit rates, as noted above, because each data stream experiences at least the same channel quality that would be experienced by a SISO system. However, in turn, require more complex receivers and transmitters to treat the information. There are several technic options for transmission and reception of the information considering MIMO systems, which are characterized by different trade-offs between performance and complexity.

Nevertheless, if we do not pay attention to certain aspects, the increase in the number of antennas can become very sparing. An important requirement for multiple antenna systems is the distance between receive and transmit antennas that implies two different perspectives. Other important aspect is the necessity of focus the beams, at the transmission and at the reception, in order to decrease the interference.

2.3 Beamforming

Beamforming is based on a spatial filtering allowing concentrate the signal and aim directly at the target [35], permitting increase SNR by blocking most of the noise outside the directions of interest. The CSI acquisition is a key ingredient in wireless communication systems, especially after the rise of the multiple antenna systems, i.e., in the MIMO case. A technique that aims to concentrate more energy in a specific direction requires that CSI to be available. In addition, the quality and quantity of the CSI available are extremely important, especially when one thinks of the transmission case. However, assuming perfect CSI is not realistic in many practical scenarios. The beamforming technique can be applied at both the transmission and reception ends. At the transmission, beamforming permits the increase of the directivity for a specific direction and to minimize the power for the other direction, by configuring the radiation pattern. At the reception, beamforming is utilized to increase and decrease the sensibility of the receptor for specific directions of interest [35].

Therefore, each BS can increase the coverage range focusing its energy toward the intended users instead of wasting it with unnecessary directions. With this technique, fewer base stations are required which means a potentially cheaper implementation offering. Beamforming allows us to extend the concept of MIMO to multiple simultaneous transmissions on the same channel, due to its increased directivity. Without beamforming, two simultaneous transmissions on the same channel would cause a collision [36]. The multipath propagation present in mobile environments can be mitigated using beamforming by constructively adding multipath to increase the strength of desired signal [37]. In addition to directivity, the radiation patterns of antennas are also characterized by their beam widths and sidelobe levels. Some important pattern lobes and beam widths are presented in Fig. 9. The Half Power Beam Width (HPBW) is the angular separation in which the magnitude of the radiation pattern decreases by 50% (-3dB) from the peak of the main lobe, which is often the parameter most commonly referred to as just beamwidth.

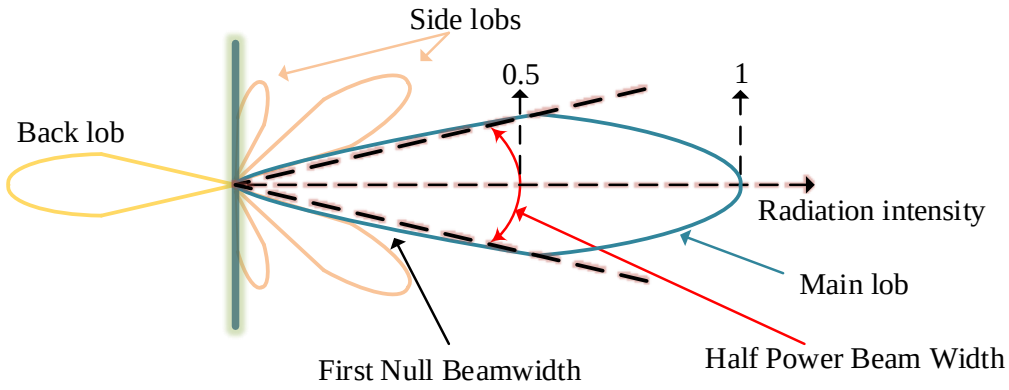

Fig. 9: Pattern lobes and beam widths.

As referred above, through beamforming techniques the beams can be produced to have high gain and low side lobes, or controlled beam width. Using an antenna array, which consists of two or more antenna elements, and beamforming technics, which permit a spatial arrange by a real-time adaptive processor, it is possible to produce a directional radiation pattern. Thus, permit yield multiple, simultaneously available beams [38]. The array factor is the most fundamental of the antenna parameters and depends on the number of elements, the element spacing, amplitude and the phase of the applied signal to each element. In [39] is shown the impact of spacing and number of elements in terms of gain and HPBW. The experience [39] demonstrated that by increasing the separation between elements and the number of elements the array factor improves, i.e., is achieved greater antenna gain and the

half power beam-width value is smaller. The separation between elements depends on the wavelength (λ), which is given by

$$\lambda = \frac{c}{f} \tag{14}$$

where f is the frequency and $c = 3*10^8\ m/s$. Thus, in order to avoid an increase in interference, the separation between each antenna element should be at least half of the wavelength:

$$d = K\lambda, \tag{15}$$

where $K \geq 1/2$. Another important antenna parameter is the effective antenna aperture, generally calculated by

$$A_e = \frac{\lambda^2}{4\pi} G = \frac{\left(\frac{c}{f}\right)^2}{4\pi} G = \frac{c^2}{4\pi f^2} G, \tag{16}$$

where G is the antenna gain. As we can see in (15) and (16), both the antenna spacing d and antenna aperture A_e depends on the frequency.

In [40] is presented the tradeoff between directivity and beam width. Through the expression of the directivity given by

$$D = \frac{T_{LA} dN_{beam}}{\lambda} = \frac{T_{LA} dN_{beam} f}{c}, \tag{17}$$

where T_{LA} depends on the type of linear array, e.g., for a broadside array $T_{LA} = 2$, which is a stacked collinear antenna consisting of half-wave dipoles spaced from one another by one-half wavelengths. The total generated beam number N_{beam} has to be less or equal than the number of transmit antennas $(N_{beam} \leq N_{tx})$. For a ULA, the expression associated to the beam width utilized in [40] is based on the Half Power Beam (HPB) and is given by

$$HPB = \frac{C\lambda}{\pi dN_{beam}} = \frac{Cc}{\pi dN_{beam} f}, \tag{18}$$

where $C = 2.782$ is a constant parameter in antenna design. Theoretically, adding more antennas (elements) can improve the beamforming performance due to the increased

directivity and also narrows down the beam width. Thus, despite the distance between antennas should be enough to obtain low correlation among channels, close distance is also required to produce a narrow beam for not generate lobes introducing interference [23].

2.4 Massive MIMO

As explained previously, the MIMO concept which means the use of multiple antennas at both transmitter and receiver increases the data throughput and link range without an additional increase in bandwidth or transmit power. Furthermore, by increasing the number of antennas greater antenna gain is achieved and it is possible to generate narrow beams and hence increase the directivity, as shown in 2.3. The massive MIMO concept uses hundreds of antennas to simultaneously serve dozens of user terminals (UT) [9]. Thus, in mMIMO the bandwidth efficiency is improved and transmitter power is reduced as it is proved in [9]. Due to the large degrees of freedom, mMIMO is capable of improving the bandwidth efficiency or the reliability by improving the multiplexing gains or diversity gains.

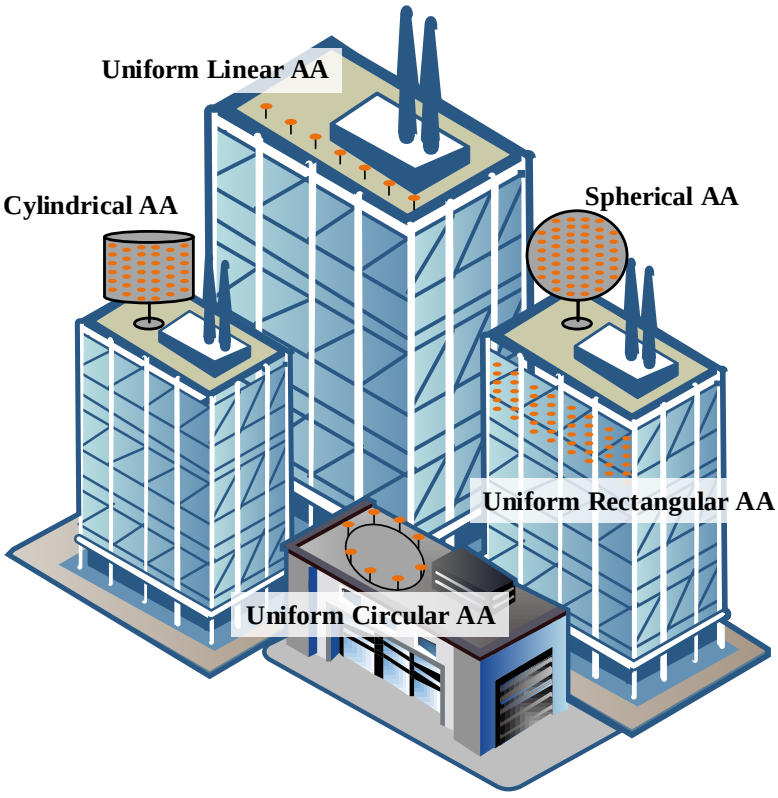

Fig. 10: Different antenna arrays configurations.

As shown in Fig. 10 an Array Antenna (AA) can be arranged with a circular form and when all adjacent antenna elements are equally separated the given designation is Uniform Circular Array (UCA). A Uniform Linear Array (ULA) consists of antenna elements equally separated on a straight line, as also shown in Fig. 10. Therefore, if the phase α_n of the feeding current to the *n*th antenna element is increased by $\alpha_n = n\alpha$, where α is a constant, then the array is referred to as a progressive phase-shift array [37]. However, both UCA and ULA can only perform one-dimensional beamforming counterpart the Uniform Planar Array (UPA) or Uniform Rectangular Array (URA), presented by Fig. 10, that can be used for two-dimensional beamforming [37]. With this new concept at both BS and UT the benefits previously presented, achieved by the increase of the number of antennas, can be reached through the use of an AA based in mMIMO. Therefore, more antennas help focus energy with an extremely narrow beam, this implies an improvement in terms of energy efficiency and a reduction of inter-user interference [9].

Despite in MIMO systems, the beam can only be adjusted in the horizontal dimension, for mMIMO based antenna arrays makes perfect sense to exploit the vertical dimension through spherical or cylindrical antenna arrays. The Fig. 10 presents these two antenna arrays which exploit the vertical dimension, jointly with the antenna arrays utilized for MIMO systems already presented in 2.3. With these arrays, we can adjust both azimuth and elevation angles, and propagate signals in Three-Dimensional (3D) space that are more realistic for practical systems. The distributed antenna array is used inside buildings and for outdoor cooperation [9].

In 2.3 we showed that to increase the number of antenna elements seems to be a viable way to reach better performances, which are needed for the future mobile systems. However, as was also discussed, the distance between different antennas should be reduced to generate narrow beams. On the other hand, the antennas must be sufficiently separated to decrease the correlation among channels. Furthermore, in addition to the distance between antenna elements, the antenna aperture also represents a limitation for the construction of the systems with several antennas, due to its dimensions. Therefore, it is impossible to design BSs or UTs with a massive number of antennas because for the frequency used by current cellular systems the antenna aperture and the space between each element implies very large structures. By (15) and (16) we can affirm that both distances between antenna elements and

antenna aperture depends on frequency and that if this parameter can be changed systems with massive number of antennas will be possible.

3 Equalization Techniques

In this dissertation, we give more importance to uplink communication since equalization is the focal point of the practical work developed. Designing more efficient equalizers in order to reduce the interference between users is one of the most important aims of future cellular systems. This chapter address both linear and non-linear digital equalization techniques that will be useful to understand the work developed in Chapter 5.

3.1 Digital Equalization Techniques

In MIMO systems, the complexity reduction of the schemes and algorithms is also associated with the quality and quantity of CSI, which is not always available. In digital communications, the aim of the equalizer is to reduce the intersymbol interference (ISI) to allow recovery of the transmit symbols.

Single carrier modulation is a traditional digital communication format, where data symbols are transmitted in serial mode, requires a single radio frequency to carry the information. Thus, the data is modulated into only one carrier, as described in Fig. 11, where the energy associated to each different symbol occupies the total transmission band.

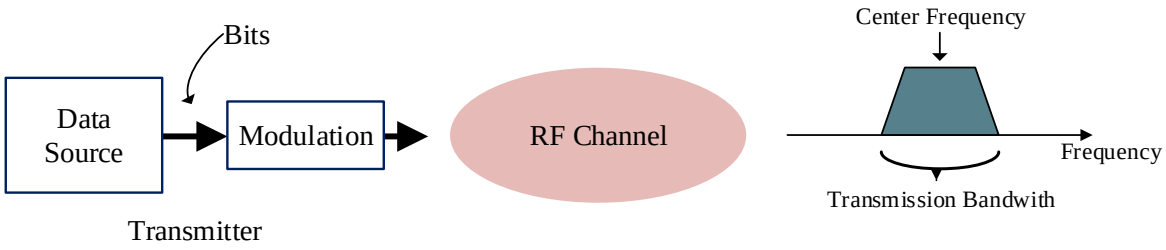

Fig. 11: Conventional single carrier transmission.

However, multicarrier modulation where multiple data streams are transmitted in parallel has an excellent complexity-performance trade-off, allowing a simpler equalization than

with the single carrier [41]. With multicarrier modulation the symbols are distributed through several different sub-carriers, using a filter bank which establishes the same spacing between each sub-carrier, as shown in Fig. 12.

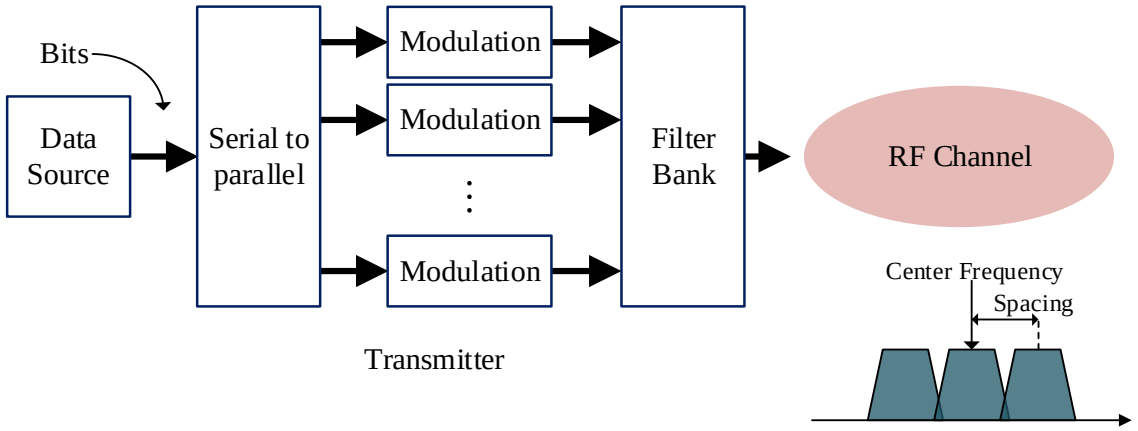

Fig. 12: Conventional multicarrier transmission.

In a multiuser environment, the equalizer must also seek to reduce interference between users. Thus, it is quite important algorithms to reduce ISI and to allow to null out the effect of the other users (interference). The linear equalizers represent a low complexity approach [42]. As shown in Fig. 13, the linear based equalizer structures have no feedback path.

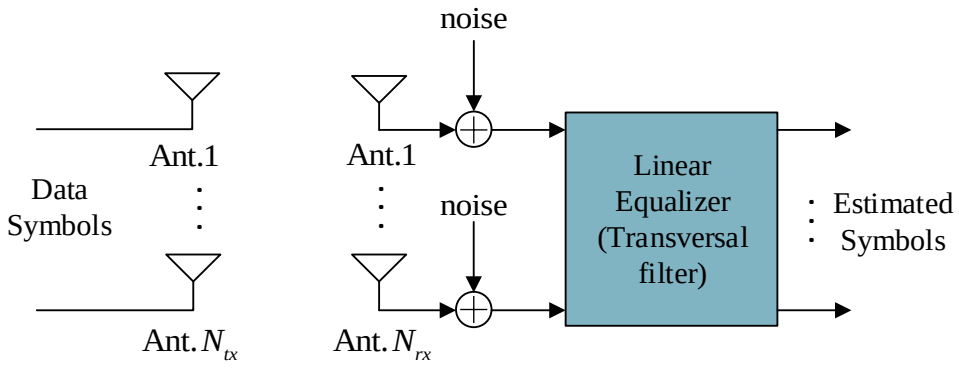

Fig. 13: Linear receiver architecture.

At the receiver side, for a given time slot, the data symbols arrive through N_{rx} antennas jointly with associated noise. Then the receiver information passes through a linear structure, which can be described as a transversal filter, allowing to compute the estimated symbols. The method to obtain the estimated data symbols depends on the algorithm that is performed by the linear structure.

These linear structures represent the most simple and common type of channel equalizer used in practice to reduce the ISI [42]. The main architectures used under linear equalizers are Zero Forcing (ZF) based equalizer and Minimum Mean Squared Error (MMSE) based equalizer. These two methods ZF and MMSE are also the building blocks of more advanced communication schemes such as the decision feedback equalizer (DFE), or equivalently, the V-BLAST (vertical Bell Labs layered Space-Time) architecture and various other MIMO transceiver designs [41].

3.2 Linear Zero Forcing Based Equalizer

The ZF architecture aims to design an equalizer vector for each data symbol to remove the interference. The name ZF corresponds to bringing down the ISI to zero in a noise free case. This will be useful when ISI is significant compared to noise [43]. The interference is removed because the equalizer vector must be orthogonal to the channels of the other symbols. A ZF linear equalizer applies the inverse of the channel frequency response to the received signal, to restore the signal after the channel [44]. Thus, the linear matrix $\mathbf{G}_{ZF}$ which removes the interference is given by

$$\mathbf{G}_{ZF} = \left(\mathbf{H}^H \mathbf{H}\right)^{-1} \mathbf{H}^H. \tag{19}$$

However, the performance of ZF linear equalizer is degraded with low SNR, i.e., the noise term $\mathbf{G}_{ZF}\mathbf{n}$ is amplified when the channel is in deep fading.

3.3 Linear Minimum Mean Square Error Based Equalizer

To minimize the ISI and additive noise effects, the equalizer coefficients can be optimized using the MMSE criterion [44]. Thus, an alternative to ZF architecture is the MMSE architecture that minimizes the mean square error between the transmitted symbol vector and its estimates at the receiver. The MSE expression is given by

$$\text{MSE}=\mathbb{E}\left[\left\|\tilde{\epsilon}\right\|^2\right], \tag{20}$$

where $\lim_{x\to\infty} \tilde{\epsilon}$ is the average error and denotes the overall error. Assuming that there is no noise $\left(SNR \to \infty\right)$ the matrix that minimizes the MSE (MMSE) can be simply an inverse of the channel matrix, presenting the same behavior as the ZF linear based equalizer [44].

However, the noise will always be present in mobile communication systems and thus it is necessary a model capable of reflecting this unwanted effect. At the optimum point, there should be no correlation between the received signal and the error. Nevertheless, the MMSE algorithm should be able to decrease (20) even more by utilizing the correlation. Considering that the matrix $\mathbf{G}_{MMSE}$ contains the MMSE equalizer vectors of each data symbol and that there is no correlation between input and noise it is possible to obtain the $\mathbf{G}_{MMSE}$ expression, as follows:

$$\mathbf{G}_{MMSE} = \mathbf{H}^H \left(\mathbf{H}\mathbf{H}^H + \frac{\sigma^2}{P} \mathbf{I}_{N_{tx}} \right)^{-1} \tag{21}$$

where P denotes the power of the transmitted signal and σ the variance of the noise. A common perception about ZF and MMSE is that ZF is the limiting form of MMSE as $SNR \to \infty$. Thus, the average capacity loss due to using the linear ZF or MMSE equalizers converges to a constant as SNR increases [43]. As shown in [43], there is a considerable gap between the performances of ZF and MMSE linear equalizers, even for different diversity-multiplexing tradeoff scenarios. The MMSE method presented in [38], for a beamforming context, provides optimum results in a multipath fading environment, utilizing reference signal correlated with the desired signal and uncorrelated with interferences. When the array output is compared with a reference signal, the produced beams acquire the direction of the multipath signal, which matches with the reference signal. Thus, for the non-line-of-sight urban environment, it not only reduces the interference but also the multipath fading is mitigated.

Nevertheless, a linear equalizer yields less than ideal performances and thus, other types of equalizers have been proposed with nonlinear structures [42].

3.4 Nonlinear/Iterative Based Equalizer

Due to the tradeoff between equalization of the channel impulse response to remove ISI and noise enhancement at the decision point, a linear equalizer yields less than ideal performance in terms of bit error rate, especially in dispersive channels [41]. Other types of equalizers have been proposed, especially ones with a nonlinear/iterative structure denoted as decision feedback equalizer. In these alternative equalizer structures, a first transversal

filter aiming at reducing the precursors of the equivalent pulse at the detection point is placed. Then, a linear feedback filter, whose input is the sequence of past detected data symbols, removes by cancellation the ISI due to postcursors. Hence, the structure is nonlinear with respect to the received signal [41].

An iterative block DFE (IB-DFE) was proposed in [45], where both the feedforward and the feedback filters are implemented in the frequency domain. Internally in each block the detection and design updated in sequence. Since detection is performed on a per-block basis, the effectiveness of the feedback to cancel interference is limited by the reliability of the detected data at the previous iteration. Therefore, the iterative process gradually increases the reliability of the detected data [41]. Nevertheless, if the initial detected data is extremely poor, this iterative process may not be able to efficiently cancel the interference. IB-DFE has been extended to several scenarios, as diversity scenarios, conventional and cooperative MIMO systems, among many others [46]-[51] and as expected it presented optimistic performances, e.g., for severely time dispersive channels with rich multipath propagation the IB-DFE has excellent performance.

Before the multiple antenna implementation, the IB-DFE existed as a SISO equalizer for block based SC transmissions, like in [41] and [45], with its main diagram shown in Fig. 14. To a given received block signal, the SISO IB-DFE algorithm would compute two sets of coefficients, the feedback and the feedforward coefficients. The feedforward coefficients aim to equalize the channel, with the knowledge of the channel information, while the feedback coefficients aim to both minimize the intersymbol interference (ISI) and the interference due to past incorrect estimations [52]. Iteratively performing this algorithm would yield a better and better estimation of that given block.

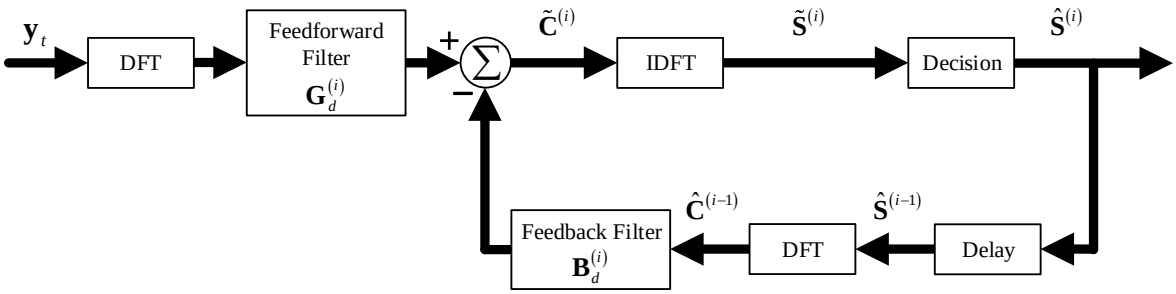

Fig. 14: IB-DFE block diagram.

Basically, a multiple antenna IB-DFE apply the successive interference cancellation (SIC) method. That is, by detecting one stream at a time and canceling the interference from already detected streams.

Let us understand the diagram shown in Fig. 14 considering a multiple antenna IB-DFE and an environment where $N_{tx} \leq N_{rx}$. For a given T-sized block, where $t \in \{1,...,T\}$, the received signal is defined as

$$\mathbf{y}_t = \mathbf{H}\mathbf{x}_t + \mathbf{n}_t . \tag{22}$$

The matrix $\mathbf{y}_t \in \mathbb{C}^{N_{rx}}$ denotes the received signal, $\mathbf{H} \in \mathbb{C}^{N_{rx}N_{tx}}$ the channel effect, $\mathbf{x}_t \in \mathbb{C}^{N_{tx}}$ the transmitted signal and $\mathbf{n}_t \in \mathbb{C}^{N_{rx}}$ the zero mean Gaussian noise vector with variance σ_n^2. It is quite important to refer that for these digital systems the number of RF chains is equal to the number of receiver antennas $\left(N_{RF} = N_{rx}\right)$. As the IB-DFE based equalizer is performed in the frequency domain, the received block signal is first processed through a Discrete Fourier Transform (DFT). At this point, we need to choose the feedforward $\mathbf{G}_d^{(i)} \in \mathbb{C}^{N_{RF} \times N_{RF}}$ and feedback $\mathbf{B}_d^{(i)} \in \mathbb{C}^{N_{RF} \times N_{RF}}$ coefficients in order to maximize the Signal-to-Interference-plus-Noise Ratio (SINR), regarding an IB-DFE receiver with hard decisions, which are defined as (23) and (24), respectively.

$$\mathbf{G}_d^{(i)} = \frac{\mathbf{H}^*}{\frac{1}{SNR} + \left(1 - \left(\rho^{(i-1)}\right)^2\right)|\mathbf{H}|^2} \tag{23}$$

$$\mathbf{B}_d^{(i)} = \rho^{(i-1)}\left(\mathbf{G}_d^{(i)}\mathbf{H} - \mathbf{I}_{N_{RF}}\right) \tag{24}$$

The correlation coefficient represented by the ρ factor is defined as

$$\rho^{(i-1)} = \frac{\mathbb{E}\left[\hat{\mathbf{S}}^{(i-1)}\hat{\mathbf{S}}^*\right]}{\mathbb{E}\left[|\mathbf{S}|^2\right]} = \frac{\mathbb{E}\left[\hat{\mathbf{C}}^{(i-1)}\hat{\mathbf{C}}^*\right]}{\mathbb{E}\left[|\mathbf{C}|^2\right]}, \tag{25}$$

which represents a measure of reliability of the estimates associated to the *i*th iteration and can be estimated as described on [53]. Relatively to the (23) expression, the SNR can be computed as

$$SNR = \frac{\sigma_s^2}{\sigma_n^2} \tag{26}$$

As represented in Fig. 14 the soft estimations at the output of the equalizer are given by the vector $\tilde{\mathbf{C}}^{(i)}$, which is obtained by

$$\tilde{\mathbf{C}}^{(i)} = \mathbf{y}\mathbf{G}_d^{(i)} - \hat{\mathbf{C}}^{(i-1)}\mathbf{B}_d^{(i)} \tag{27}$$

The vector $\hat{\mathbf{C}}^{(i-1)}$ represents the DFT of the detected output $\hat{\mathbf{S}}^{(i-1)}$. The hard decision associated with a digital modulation process, as the quadrature phase shift keying (QPSK) modulation, is represented by $\hat{\mathbf{S}}^{(i)}$.

Usually, the average received power is the quality measure chosen to rank the streams and then to identify the streams from the best to the worst. Performing the equalization in the frequency domain, this algorithm minimizes the interference between streams at each iteration, with both feedback and feedforward filters. Furthermore, it is desired to apply more than one iteration per block, in order to successfully detect all the streams.

4 Millimeter Wave Communication

As discussed in Chapter 2, the frequency is a limited resource for the current systems. Enabling the millimeter wave communications, where the spectrum is less crowded allows greater bandwidths available, as well as providing very high throughput. In this chapter, we present the millimeter wave technology that can be used to overcome the limited bandwidth constraint, associated to the current cellular systems. However, with the increase of utilized frequency band some issues about propagation, channel model and hardware rise up. This chapter will present these questions as well as the proposed solutions.

4.1 Spectrum

Today, almost all mobile communication systems use the spectrum below 3 GHz. Then, with the increasing demand for better capacity, reliability and throughput, the spectrum below 3 GHz is not able to satisfy future demands of the 5G systems. As shown in Fig. 15, mmWave communications are based on the exploitation of the 3-300 GHz band spectrum and therefore the problem of limited available bandwidth is apparently solved.

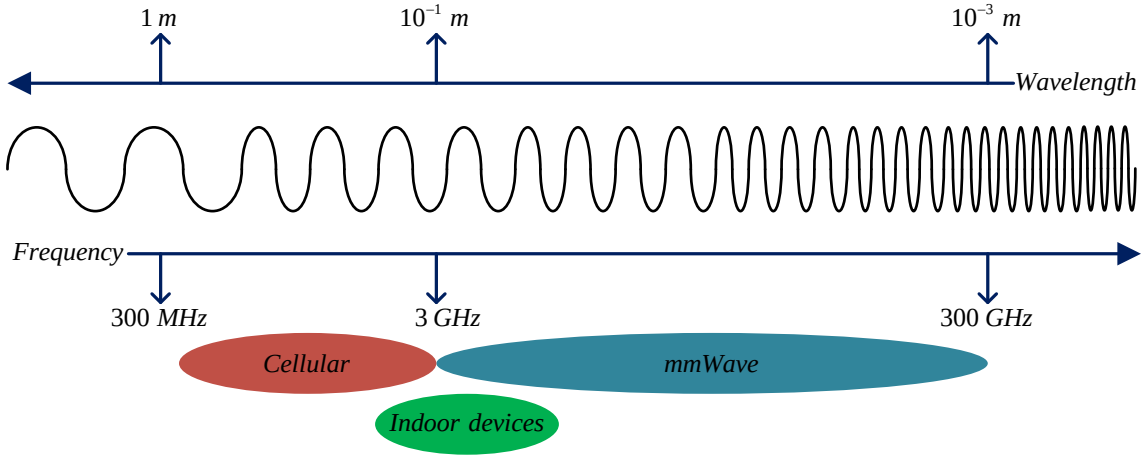

Fig. 15: Millimeter wave spectrum.

In World Radiocommunications Conferences (WRC) was discussed the possibility of allocating mmWave bands for 5G. Some of the bands discussed were 6 GHz, 18 GHz, 28 GHz, 48 GHz, 60 GHz or 70 GHz, with contiguous 300 MHz of spectrum [6].

There are already some protocols designed to explore the large bandwidth in the mmWave band to reach very high transmission rates, for indoor environments. With the 802.11n and 802.11ac protocols, which communications at 5 GHz, allows achieving significantly higher maximum data rates, when compared with the older protocols (2.4 GHz) [54]. The first IEEE wireless standard for data rates over 1 Gbit/s was the 802.15.3c, using 57-66 GHz band [12]. In [12] were tested 3 modes for this protocol and with the video streaming and multivideo streaming mode the 802.15.3c allowed to reach 3.8 Gbit/s for video streaming and multivideo streaming. More recently, the 802.11ad protocol resulted from research works when trying to achieve multigigabit speed levels (up to 7 Gbit/s) on WLANs, using signal transmission at 60 GHz [13]. However, the constraint associated to these protocols based on mmWave is the fact that they are only available for short-range services and normally designed for enclosed spaces.

4.2 Propagation

The transition to the mmWave band is a necessity nowadays but the good characteristics associated with the high-frequency communication have been known for some years, however the existing technology did not allow us to build systems with such advantages. Presently, mmWave communication already exists for WLANs enjoying not only the free spectrum but also the possibility of achieving very high transmission rates, in the order of the multigigabit [12],[13].

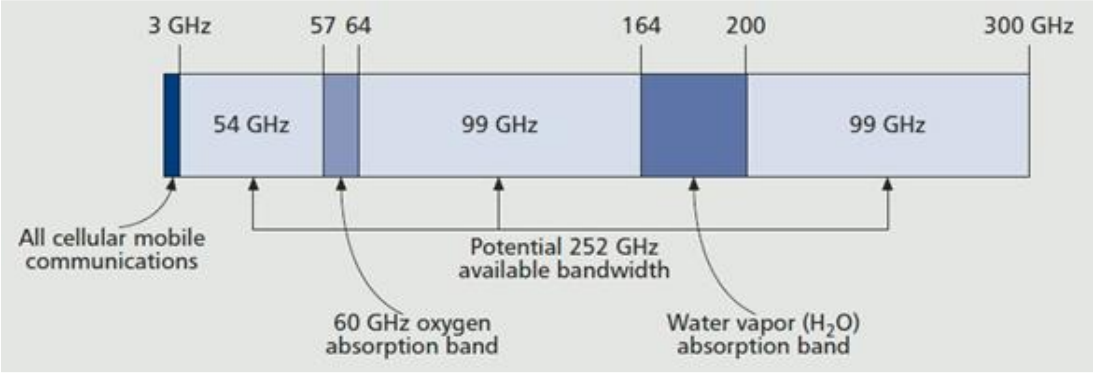

Fig. 16: Millimeter wave bands with high attenuation [55].

Nevertheless, for these cases the mmWave spectrum has been explored for short range and fixed wireless communications. Currently, there is some knowledge about mmWave propagation in indoor or outdoor environments. As shown in Fig. 16 there are two principal frequency bands where the attenuation is critical.

The oxygen molecule (O_2) absorbs electromagnetic energy near the 60 GHz frequency, thus the range 57-64 GHz represents a frequency band where we have to be careful. The attenuation, caused by the absorption of energy due to the O_2 can achieve 15 dB/Km [56]. However, there are another band where the attenuation is considerably high. The water vapour (H_2O) absorption band 164-200 GHz, depends on the quantity of H_2O and can achieve tens of dBs [56]. These two principal bands are also identified in Fig. 17, jointly with other frequency bands where the attenuation is much lower and the communication is possible. Furthermore, in urban environments the cells are on the order of 200 m [3], thereby the limitations relative to the absorption will not be a deterrent factor in relation to the path loss. In this case, the attenuation caused by atmospheric absorption is 0.012 dB at 28 GHz, 0.016 dB at 38 GHz and 0.04 dB between 80 GHz and 100 GHz [3].

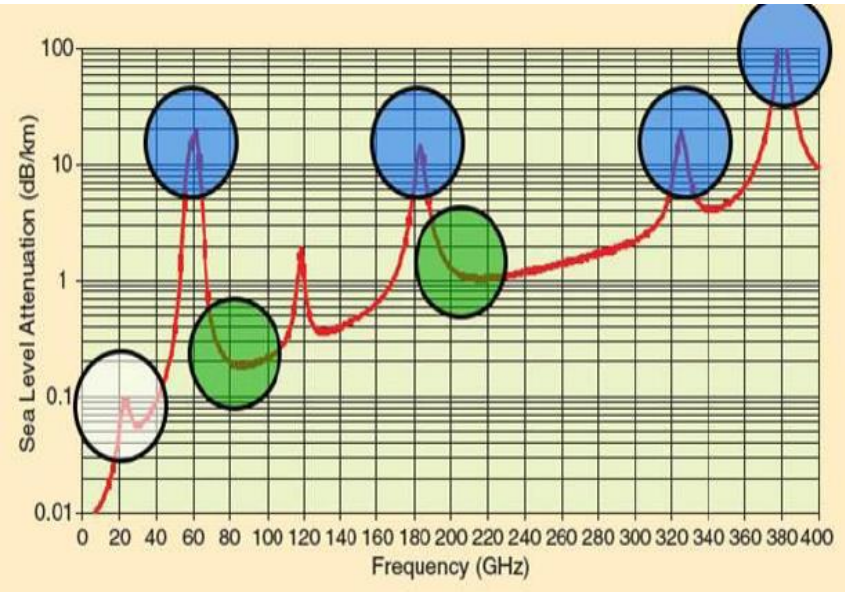

Fig. 17: Atmospheric absorption in dB/km [3].

Fig. 17 represents this behavior and it is possible to verify that for the range 80-100 GHz the attenuation is around 0.2 dB and for the range 220-240 GHz is about 1 dB. Furthermore, signals at higher frequencies cannot penetrate easily through buildings,

contrary to the signals at lower frequencies. MmWave signals do not penetrate most solid materials very well, for example, considering a signal crossing concrete material with 10 cm of thickness, which is present in the majority of the homes and other constructions, represents an attenuation of 175 dB for 40 GHz [56]. As a comparison term, for the last example, a signal below 3 GHz suffers an attenuation of 17.7 dB [56].

4.3 Millimeter Wave MIMO Channel Model

With the emergence of the mmWave communications and due to the evident differences for sub-6 GHz communications, it was necessary to study new channel models. This section briefly describes the clustered sparse mmWave channel model discussed in [16], assuming a channel that remains constant during a block but varies independently between blocks, i.e., a *T*-size block fading channel. Considering that $\mathbf{H}_u \in \mathbb{C}^{N_{rx} \times N_{tx}}$ is the channel matrix, of the *u*th user, which contributes the sum of N_{cl} clusters, each one with the contribution of N_{ray} propagation paths and that the channel has the model of Fig. 18-a) then, this channel model can be expressed mathematically as follows:

$$\begin{aligned}\mathbf{H}_u = \gamma \sum_{j,l} \alpha_{jl,u} \Lambda_{rx,u}\left(\phi_{jl}^{rx,u}, \theta_{jl}^{rx,u}\right) \Lambda_{tx,u}\left(\phi_{jl}^{tx,u}, \theta_{jl}^{tx,u}\right) \times \\ \mathbf{a}_{rx,u}\left(\phi_{jl}^{rx,u}, \theta_{jl}^{rx,u}\right) \mathbf{a}_{tx,u}\left(\phi_{jl}^{tx,u}, \theta_{jl}^{tx,u}\right)^H .\end{aligned} \tag{28}$$

where $\gamma = \sqrt{N_{tx} N_{rx} / N_{cl} N_{ray}}$ is a normalization factor, and $\alpha_{il,u}$ is the complex gain of the *l*th ray in the *i*th scattering cluster. The functions $\Lambda_{rx,u}\left(\phi_{jl}^{rx,u}, \theta_{jl}^{rx,u}\right)$ and $\Lambda_{tx,u}\left(\phi_{jl}^{tx,u}, \theta_{jl}^{tx,u}\right)$ represent transmit and receive antenna element gain for $\phi_{jl}^{rx,u}\left(\theta_{jl}^{rx,u}\right)$ and $\phi_{jl}^{tx,u}\left(\theta_{jl}^{tx,u}\right)$, i.e., the azimuth (elevation) angles of arrival and departure. The azimuth and elevation angles may be seen in Fig. 18-b). The vectors $\mathbf{a}_{rx,u}\left(\phi_{jl}^{rx,u}, \theta_{jl}^{rx,u}\right)$ and $\mathbf{a}_{tx,u}\left(\phi_{jl}^{tx,u}, \theta_{jl}^{tx,u}\right)$ represent the normalized receive and transmit array response vectors for the corresponding angles.

The manuscript [16] addressed the random distributions used to generate the path gains and the angles of the channel, such that $\mathbb{E}\left[\left\|\mathbf{H}_u\right\|_F^2\right] = N_{rx} N_{tx}$. Each AA type has its own array response vector, e.g., for a ULA on the y-axis, with N elements, the array response

vector is given by (29). For a uniform planar array (UPA) in the yz-plane with N_y and N_x elements on the y and z axes respectively, the array response vector is given by eq. (30).

$$\mathbf{a}_{ULA}(\phi) = \frac{1}{\sqrt{N_y}}\left[1, e^{j1kd\sin(\phi)}, e^{j2kd\sin(\phi)}, ..., e^{j(N_y-1)kd\sin(\phi)}\right]^T \tag{29}$$

$$\mathbf{a}_{UPA}(\phi,\theta) = \frac{1}{\sqrt{N_y N_x}}\left[1, ..., e^{jkd\{m\sin(\phi)\sin(\theta)+n\cos(\theta)\}}, ..., e^{jkd\{(N_y-1)\sin(\phi)\sin(\theta)+(N_x-1)\cos(\theta)\}}\right]^T \tag{30}$$

Where $k = 2\pi/\lambda$, d is the inter-element spacing and $0 \le m < N_y$ and $0 \le n < N_x$ [16].

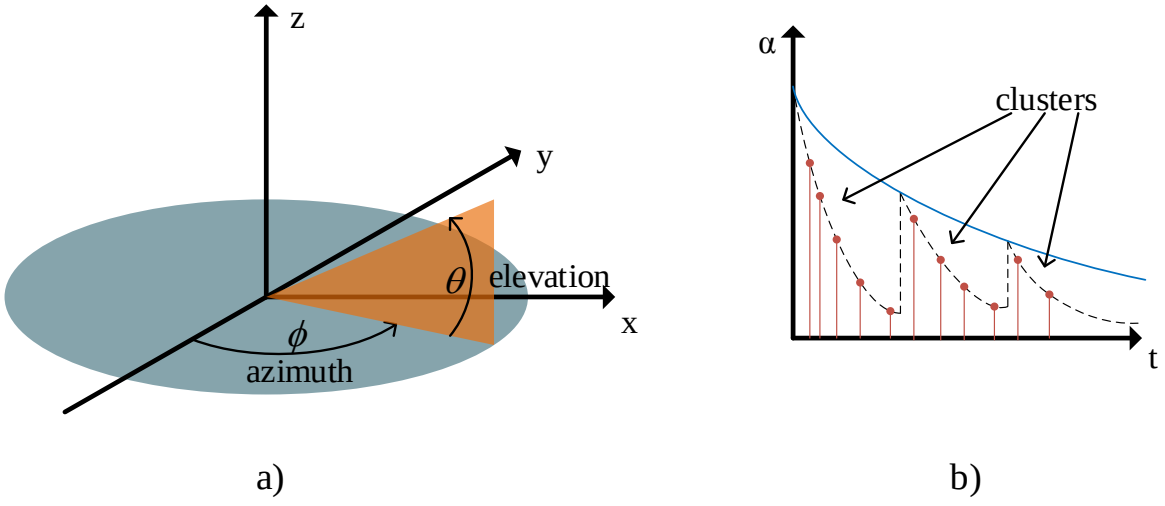

Fig. 18:a) Azimuth and elevation angles; b) clustered channel model representation.

4.4 System based on mMIMO and mmWave technologies

Since it is possible to use technology that allows the use of millimeter waveband frequencies, then the construction of systems with a massive number of antennas is also possible. As we saw in section 2.4, in order to be able, the construction of a system with a large number of antennas (mMIMO), it would be necessary to reduce the distance between consecutive antenna elements, as well as the size of the antenna aperture. Thinking in the antenna space, e.g., in the 60 GHz band, by (14) the corresponding wavelength is 0.5 cm. Hence, an AA with a large number of antenna elements having the distance $\lambda/2$ between elements may accommodate as many as 40 antennas within a physical space of 10 cm [9].

Due to the increasing the number of UTs and their traffic in urban environments, increased system capacity is required for supporting customer requirements. Currently, the

sectorization techniques that are used for providing services to several UTs, simply divide a cell into multiple sectors, increasing network capacity. However, although sectorization is capable of improving the area bandwidth efficiency, this benefit comes at the expense of a potentially increased interference among sectors, due to the none ideal antenna patterns [9]. Therefore, more efficient techniques are required to further increase the achievable network capacity. As illustrated in Fig. 19, in mMIMO systems can be achieved an accurate sectorization, through high selectivity angular beamforming. This high selectivity angular beamforming performed horizontally, is capable of reducing the interference among sectors. Moreover, the coverage of each beam can be changed by adjusting the elevation angle of 3D beamforming [9]. By this way, a conventional fixed sector can be further splitted into inner and outer sectors, each of which can be served by a 3D Beamformer (BF) with the same horizontal but different elevation angles [9]. The same frequency radio resources can be reused by all the sectors, then, it is possible to significantly increase the number of UTs served and/or of improving the network's throughput.

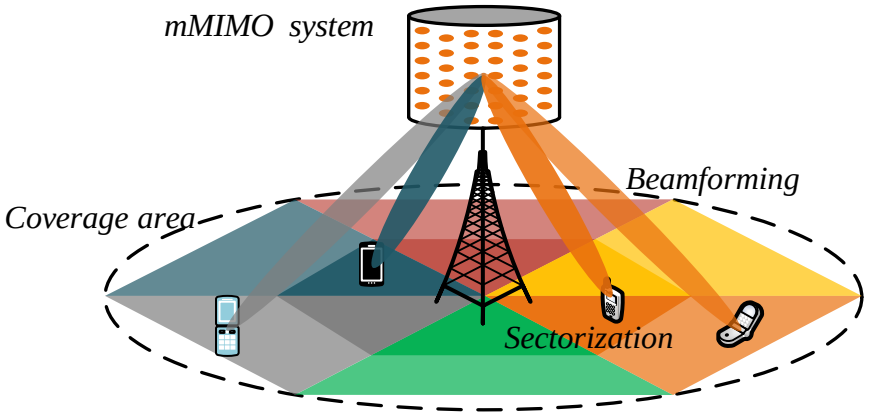

Fig. 19: Ilustration of a mmWave mMIMO based system with multi-layer sectorization.

4.5 Millimeter Wave Massive MIMO Architectures

To overcome the challenges like severe path loss, penetration loss or rain fading, mmWave require very high gain antenna systems. It is known that mmWave frequencies are already used for outdoor point-to-point backhaul links, however, to achieve these very high gains a large physical aperture antenna is used, which is not economically advantageous [57]. As referred in [8] the valid option is to use mMIMO technology for mmWave frequency applications. Thus, using mmWave bands several tens of GHz of bandwidth become available for wireless systems [58], while mMIMO allows the continued increasing demand

for higher data rates for future wireless networks [59]. Therefore, mmWave and mMIMO are considered as two of the key enabling technologies needed to meet the QoS requirements for future wireless communication [60]. With mmWave mMIMO combination arises the possibility of exploiting new efficient spatial processing techniques, such as beamforming/precoding and spatial multiplexing at both transmitter and/or receiver terminals [61]. Inevitably the techniques used in these systems are different than those used for sub-6 GHz, due to the high limitations in hardware [57]. The fully digital precoding/combining architectures, used for sub-6 GHz, reach an optimum performance, however, in these systems one RF chain is required for each antenna element, at the BS and at the UT. When the number of antennas is very large, like in mmWave mMIMO systems, it is not practical to have one fully dedicated RF chain by each antenna [62], due to the power consumption and the high cost of mmWave mixed-signal components. On the other hand, the performance of the purely analog techniques, proposed in [63], [64] is limited by constraints on the amplitudes of phase shifters and due to the phases of the ones quantized. Therefore, analog beamforming is usually limited to single-stream transmission [65]. These limitations are overcome by doing some signal processing at an analog level and the rest at the digital level, that are called hybrid analog/digital architectures and have been addressed in [65],[66].

In the hybrid analog/digital architecture, the transmitter and receiver processing are divided between the analog and digital domains. This division approach allows that the number of RF transmit/receive chains to be lower than the number of transmit/receive antennas. In these architectures, it is possible to connect each of the RF chains to many receive and transmit antennas.

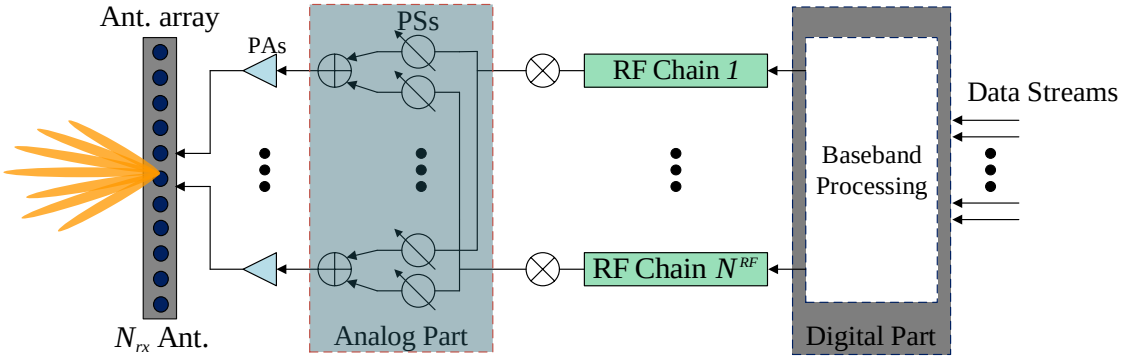

Fig. 20: Base Station with the fully connected hybrid analog/digital architecture.

The analog beamforming includes a single RF chain and one analog phase weight per antenna element to obtain the maximum gain in the direction of the dominant channel paths. The amplitude of a phase shifter is constant therefore, it has degraded performance when compared to digital beamforming. Thus, it becomes difficult to control the signal amplitude and the phase of the low-resolution signal. In [19]-[21] some beamforming approaches have been proposed with a fully connected hybrid architecture, for multiuser systems. In the fully connected approach each antenna element is connected with all RF chains, as shown in Fig. 20. Nevertheless, as this architecture is dedicated to the mMIMO systems, it involves a high effort due to its structural and computational complexity, i.e., the total number of the RF paths which is necessary to control is given by $N_{rx}N^{RF}$.

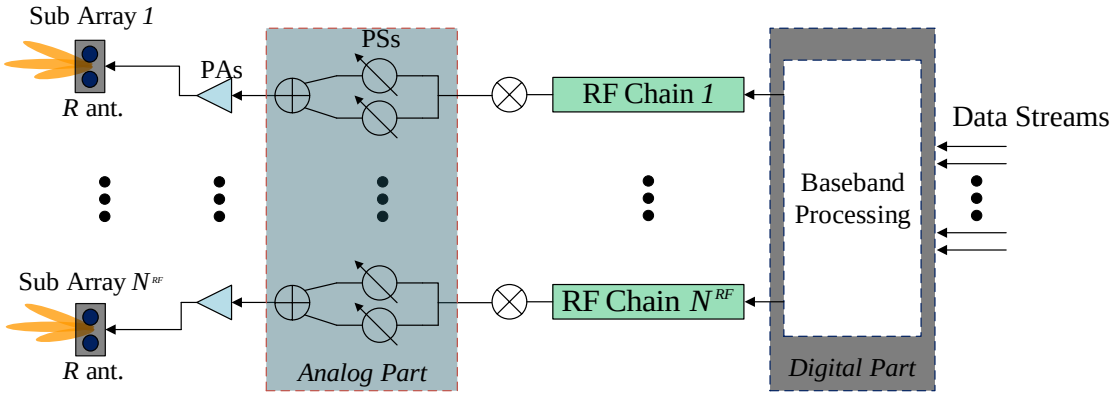

Fig. 21: Base station with the sub-connected hybrid analog/digital architecture.

In addition to the fully connected architectures, the sub-connected architectures are considered because they allow a reduction of the number of PSs from $N_{rx}N^{RF}$ to N_{rx}, when compared with fully connected counterparts [22],[67]. Therefore, the power consumption used to excite and to compensate the insertion loss of PSs is reduced, and the computational complexity is also lower [22]. The sub-connected hybrid architecture represented in the Fig. 21 results in simplicity of the circuits represents lower cost and achieves better energy efficiency [16]. This hybrid architecture also provides a lower spectral efficiency when compared with the fully-connected case [67].

The sub-connected architectures can be divided into two types, dynamic and fixed [68], as identified in Fig. 22. In the dynamic sub-connected structure, each RF chain can dynamically connect to a different set of antennas. On the other hand, in the fixed sub-connected case each RF chain is permanently connected to the same set of antennas [69].

Transmit/receive analog beamforming are jointly computed in the first stage to maximize the power of the desired signal, and then, the interference is explicitly mitigated in the digital domain.

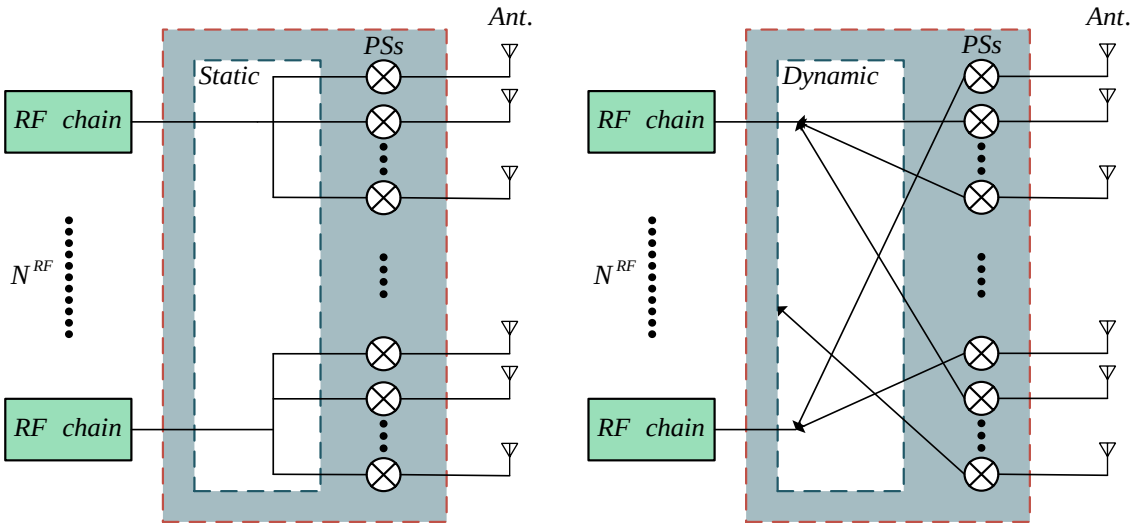

Fig. 22: Sub-connected analog RF precoder/combiner for both cases, Static and Dynamic.

5 Iterative Multiuser Equalization for Sub-Connected Hybrid mmWave Massive MIMO Systems

The new generation of cellular network (5G) is coming, and some innovative technologies are needed to assure better performance and QoS. As previously mentioned, mMIMO and mmWave communications are two enabling technologies to meet the QoS requirements for 5G. With mmWave bands, several tens of GHz of bandwidth become available, while the mMIMO allows the continued increasing demand of higher data rates. However, in these systems it is not practical to have one fully dedicated RF chain per antenna (fully digital case) due to the power consumption and high cost of mmWave mixed-signal components. On the other hand, the pure-analog techniques are limited by the constraints of practical PSs, which have unit amplitude and whose phases can be configured only in a discrete set of values. These limitations are overcome by the so called hybrid analog/digital architectures where some signal processing is done at the analog level and the rest at the digital level. As discussed in chapter 4, in addition to the fully connected architectures, there are the sub-connected architectures that allow us to reduce the number of PSs. Thus, the power consumption used to excite and to compensate the insertion loss of PSs is reduced, and the computational complexity is also lower [22]. The limitation that each RF chain is only physically connected to a subset of antennas makes the design of the proposed sub-connected hybrid iterative multiuser equalizer harder than for the fully connected based approaches. In this chapter, the design of the hybrid iterative space-time feedback equalizer with sub-connected architecture is optimized by using the average bit-error-rate (BER) as a metric. The analog part of the equalizer is computed sequentially over the RF chains using a dictionary built from the array response vectors. The study of BER performance of the

proposed sub-connected hybrid iterative multiuser equalizer when the number of iterations increases is also an important aspect of this work.

5.1 System Characterization

In the next two sub-sections we present the system characterization which comprises the transmitter and receiver model description. For each UT, i.e. the transmitter, we consider a model with low complexity and without the knowledge of CSI before transmission. The low complexity terminal has only one RF chain. At the BS, i.e. the receiver, we design a hybrid analog/digital equalizer, with static sub-connected architecture.

5.1.1 User-Terminal Model Description

Each UT has only a single RF chain and sends only one data stream per time slot, over the N_{tx} transmit antennas, as shown in Fig. 23. To simplify the overall system design we assume that the UTs have no access to CSI. The analog precoder of *u*th UT at the instant *t* is mathematically modeled by $\mathbf{f}_{a,u,t} \in \mathbb{C}^{N_{tx}}$ and is physically realized using a vector of analog PSs, where all elements of the vector $\mathbf{f}_{a,u,t}$ have equal norm $(|\mathbf{f}_{a,u,t}(l)|^2 = N_{tx}^{-1})$. In the following we consider a low complexity UT, which is the analog precoder of the *u*th UT at the instant *t* is generated randomly accordingly to

$$\mathbf{f}_{a,u,t} = \left[e^{j2\pi\phi_n^{u,t}} \right]_{1\le n\le N_{tx}, 1\le t\le T}, \tag{31}$$

where $\phi_n^{u,t}$ with $n \in \{1,...,N_{tx}\}$, $t \in \{1,...,T\}$ and $u \in \{1,...,U\}$ are i.i.d. uniform random variables such that $\phi_n^{u,t} \in [0,1]$. To guarantee that the transmit signal and then the noise plus interference are Gaussian distributed at the receiver side, the transmit signal $\mathbf{X}_u = [\mathbf{x}_{u,1},...,\mathbf{x}_{u,T}]$ is built by using a STBC. A Discrete Fourier Transform performs the time, and the analog precoder performs the space encoding. The STBC simplifies the receiver optimization and increases the diversity of the mmWave mMIMO system. Mathematically, the operation is expressed by

$$\mathbf{x}_{u,t} = \mathbf{f}_{a,u,t} c_{t,u}, \tag{32}$$

$$\mathbf{c}_u^T = \mathbf{s}_u^T \mathbf{W}_T \,, \tag{33}$$

where $\mathbf{W}_T \in \mathbb{C}^{T\times T}$ denotes a *T*-point DFT matrix and $\mathbf{c}_u = \left[c_{t,u} \right]_{1\le t\le T}$ the time encoded version of $\mathbf{s}_u = \left[s_{t,u} \right]_{1\le t\le T} \in \mathbb{C}^T$. The vector $s_{t,u}, t \in \{1,...,T\}$ designates a complex data symbol selected from a quadrature amplitude modulation (QAM) constellation with $\mathbb{E}\left[\left| s_{t,u} \right|^2 \right] = \sigma_u^2$, where $\sum_{u=1}^{U} \sigma_u^2 = U$. The transmitter total power constraint is $\left\| \mathbf{X}_u \right\|_F^2 = T$. For the sake of simplicity, and without loss of generality, in this work, only QPSK constellations are considered.

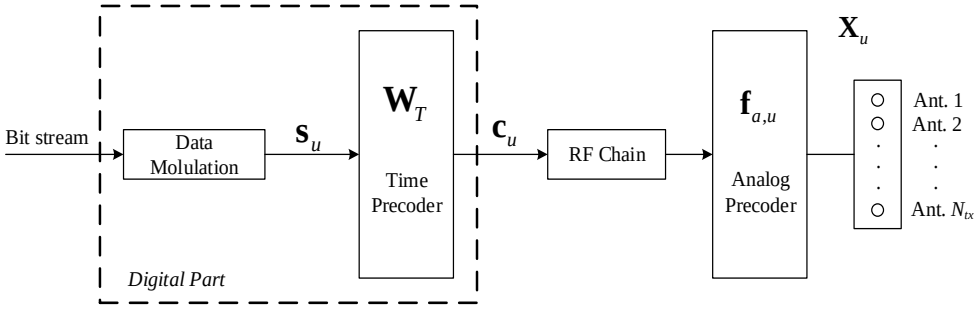

Fig. 23: User-terminal (UT) block diagram.

5.1.2 Receiver Model Description

The main objective of this research was to design a hybrid receiver with sub-connected architecture, which was based on two distinct parts, the analog and the digital parts. For a given *T*-sized block, the received signal is given by

$$\mathbf{y}_t = \sum_{u=1}^{U} \mathbf{H}_u \mathbf{x}_{u,t} + \mathbf{n}_t, \tag{34}$$

where $\mathbf{y}_t \in \mathbb{C}^{N_{rx}}$ denotes the received signal vector and $\mathbf{n}_t \in \mathbb{C}^{N_{rx}}$ the zero mean Gaussian noise vector with variance σ_n^2. This signal is processed at the receiver by an iterative block decoder based on the sub-connected hybrid architecture, as seen in Fig. 24. First, the received signal $\mathbf{y}_t$ is processed through the phase shifters in the analog part, modeled by the vector $\mathbf{g}_{a,p,t} \in \mathbb{C}^R$, where $p \in \left\{1,...,N_{rx}^{RF}\right\}$ represents the index of the RF chain connected to a set of

$R = N_{rx} / N_{rx}^{RF}$ antennas. The global analog matrix $\mathbf{G}_{a,t} \in \mathbb{C}^{N_{rx}^{RF} \times N_{rx}}$ has the following block-diagonal structure

$$\mathbf{G}_{a,t} = \begin{bmatrix} \mathbf{g}_{a,1,t}^T & 0 & 0 & 0 & 0 \\ 0 & \ddots & 0 & 0 & 0 \\ 0 & 0 & \mathbf{g}_{a,p,t}^T & 0 & 0 \\ 0 & 0 & 0 & \ddots & 0 \\ 0 & 0 & 0 & 0 & \mathbf{g}_{a,N_{RF},t}^T \end{bmatrix}. \tag{35}$$

The baseband processing contains N_{rx}^{RF} chains, each one connected to a subset of R antennas, and a closed-loop comprising a digital forward and a feedback path. All elements of the vectors $\mathbf{g}_{a,p,t}$ have equal norms $\left(\left| \mathbf{g}_{a,p,t}(l) \right|^2 = N_{rx}^{-1} \right)$. For the digital forward path, the signal first passes through a linear filter $\mathbf{G}_{d,t} \in \mathbb{C}^{U \times N_{rx}^{RF}}$ then follows a time equalizer and decoding. In the digital feedback path, the recovered data from the forward path first passes through the time precoder and then through the feedback matrix $\mathbf{B}_{d,t} = \left[\mathbf{b}_{d,1,t}, ..., \mathbf{b}_{d,U,t} \right] \in \mathbb{C}^{U \times U}$. The time encoding and decoding of the data symbols obeys (33) and

$$\tilde{\mathbf{S}} = \tilde{\mathbf{C}} \mathbf{W}_T^H , \tag{36}$$

where the codeword matrix $\tilde{\mathbf{C}} = \left[\tilde{\mathbf{c}}_1, ..., \tilde{\mathbf{c}}_T \right]$, $\tilde{\mathbf{c}}_t = \left[\tilde{c}_{u,t} \right]_{1 \le u \le U}$ is a soft estimate of transmitted symbols. Both feedback and feedforward paths are combined; the signal output of the feedback path is subtracted from the filtered received signal $\mathbf{G}_{d,t} \mathbf{G}_{a,t} \mathbf{y}_t$.

This proposed receiver structure is a sub-connected hybrid iterative feedback multiuser equalizer, where the main difference from the conventional iterative block decision feedback based equalizers is the analog front-end of constant amplitude phase shifters with sub-connected architecture. The limitation that all elements of each analog vector must have the same norm and furthermore the structure imposed by the sub-connected architecture makes the design of the proposed equalizer harder than for the conventional fully digital or even the hybrid analog/digital full-connected architectures. When compared with the fully connected hybrid architecture the sub-connected hybrid architecture, where only a set of antennas is connected to each RF chain, simplifies the physical implementation.

In the following sections the analog and digital forward matrices, $\mathbf{G}_{a,t}$ and $\mathbf{G}_{d,t}$ are designed as well as the digital feedback matrix $\mathbf{B}_{d,t}$.

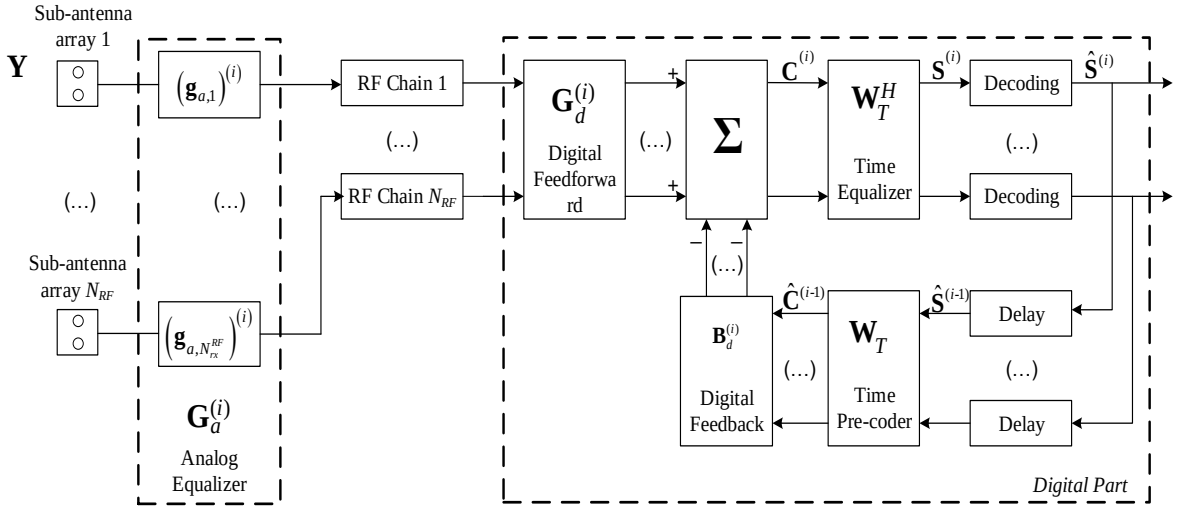

Fig. 24: Hybrid Iterative Multiuser Equalizer for sub-Connected Architecture.

5.2 Iterative Receiver Design

In this section, the proposed hybrid iterative multiuser equalizer is derived for the sub-connected mmWave mMIMO based systems, discussed in the previous section. It was assumed a decoupled joint transmitter-receiver optimization problem, with the focus on the design of the sub-connected hybrid multiuser equalizer.

5.2.1 MSE Calculation

A block diagram of the proposed iterative multiuser equalizer is shown in Fig. 24. The received signal corresponding to user u at the *t*th time slot for the *i*th iteration is given by

$$\tilde{c}_{u,t}^{(i)} = \sum_{p=1}^{N_{rx}^{RF}} g_{d,up,t}^{(i)} \left(\mathbf{g}_{a,p,t}^{(i)}\right)^T \mathbf{y}_{p,t} - \left(\mathbf{b}_{d,u,t}^{(i)}\right)^T \hat{\mathbf{c}}_t^{(i-1)}, \tag{37}$$

where $g_{d,up,t}^{(i)} = \mathbf{G}_{d,t}^{(i)}(u,p)$ is the element of *u*th row and *p*th column of $\mathbf{G}_{d,t}^{(i)}$, $\mathbf{g}_{a,p,t}^{(i)} \in \mathbb{C}^R$ denotes the analog part of the feedforward vector of user p, $\mathbf{y}_{p,t} = \left[\mathbf{y}_t(j)\right]_{R(p-1)+1 \le j \le Rp}$, $\mathbf{b}_{d,u,t}^{(i)} \in \mathbb{C}^U$ is the feedback vector of user u, and $\hat{\mathbf{c}}_t = \left[\hat{c}_{u,t}\right]_{1 \le u \le U} \in \mathbb{C}^U$ is the estimate of the

transmitted symbols. The matrix $\hat{\mathbf{C}}^{(i-1)} = \left[\hat{\mathbf{c}}_1^{(i-1)},...,\hat{\mathbf{c}}_T^{(i-1)}\right] \in \mathbb{C}^{U\times T}$ is the DFT of the detector output $\hat{\mathbf{S}}^{(i-1)}$, performed by de time precoder $\mathbf{W}_T$. The hard decision related with the QPSK data symbols $\mathbf{S} = \left[\mathbf{s}_1,...,\mathbf{s}_t,...,\mathbf{s}_T\right]$ is $\hat{\mathbf{S}}^{(i)} = \left[\hat{\mathbf{s}}_1,...,\hat{\mathbf{s}}_t,...,\hat{\mathbf{s}}_T\right]$. At the iteration *i*, the hard decision $\hat{\mathbf{s}}^{(i)}$ is achieved through the sign of $\tilde{\mathbf{s}}^{(i)}$, for QPSK constellations. From the central limit theorem, $\mathbf{c}_t = \left[c_{u,t}\right]_{1\le u\le U}$, $u \in \{1,...,U\}$, $t \in \{1,...,T\}$ is approximately Gaussian distributed. In addition, since the input-output relationship between $\mathbf{c}_t$ and $\hat{\mathbf{c}}_t^{(i)}$, $u \in \{1,...,U\}$, $t \in \{1,...,T\}$ is memoryless, by the Bussgang theorem [70] applies and follows,

$$\hat{\mathbf{c}}_t^{(i)} = \boldsymbol{\Psi}^{(i)}\mathbf{c}_t + \hat{\epsilon}_t^{(i)},\ t \in \{1,...,T\}, \tag{38}$$

where $\boldsymbol{\Psi}^{(i)}$ is a diagonal matrix given by

$$\boldsymbol{\Psi}^{(i)} = \mathrm{diag}\left(\psi_1^{(i)},\ldots,\psi_u^{(i)},\ldots,\psi_U^{(i)}\right), \tag{39}$$

$$\psi_u^{(i)} = \frac{\mathbb{E}\left[\hat{\mathbf{c}}_t^{(i)}(u)\mathbf{c}_t^*(u)\right]}{\mathbb{E}\left[|\,\mathbf{c}_t(u)\,|^2\right]}, u \in \{1,\ldots,U\}, \tag{40}$$

and $\hat{\epsilon}_t^{(i)}$ is an error vector with zero mean and uncorrelated with $\mathbf{c}_t$, $t \in \{1,...,T\}$, as described in [21] and [71]. Let us consider $\bar{\mathbf{H}}_{p,t} = \left[\mathbf{H}_t(j,l)\right]_{R(p-1)+1\le j\le Rp,1\le l\le U} \in \mathbb{C}^{R\times U}$ and $\mathbf{H}_t = \left[\mathbf{H}_1\mathbf{f}_{a,1,t},...,\mathbf{H}_U\mathbf{f}_{a,U,t}\right] \in \mathbb{C}^{N_{rx}\times U}$; therefore, from (37) and (38), it follows that

$$\begin{aligned}\tilde{c}_{u,t}^{(i)} &= \sum_{p=1}^{N_{rx}^{RF}}\left[g_{d,up,t}^{(i)}\left(\mathbf{g}_{a,p,t}^{(i)}\right)^T\left(\bar{\mathbf{H}}_{p,t}\mathbf{c}_t + \mathbf{n}_{p,t}\right)\right] - \left(\mathbf{b}_{d,u,t}^{(i)}\right)^T\left(\boldsymbol{\Psi}^{(i-1)}\mathbf{c}_t + \hat{\epsilon}_t^{(i-1)}\right)\\ &= \sum_{p=1}^{N_{rx}^{RF}}\left[g_{d,up,t}^{(i)}\left(\mathbf{g}_{a,p,t}^{(i)}\right)^T\bar{\mathbf{H}}_{p,t}\mathbf{c}_t\right] + \sum_{p=1}^{N_{rx}^{RF}}\left[g_{d,up,t}^{(i)}\left(\mathbf{g}_{a,p,t}^{(i)}\right)^T\mathbf{n}_{p,t}\right]\\ &\quad - \left(\mathbf{b}_{d,u,t}^{(i)}\right)^T\boldsymbol{\Psi}^{(i-1)}\mathbf{c}_t - \left(\mathbf{b}_{d,u,t}^{(i)}\right)^T\hat{\epsilon}_t^{(i-1)},\end{aligned} \tag{41}$$

where $\mathbf{n}_{u,t} = \left[\mathbf{n}_t(j)\right]_{R(u-1)+1\le j\le Ru} \in \mathbb{C}^R$. Define $\mathbf{g}_{ad,up,t}^{(i)} = g_{d,up,t}^{(i)}\mathbf{g}_{a,p,t}^{(i)} \in \mathbb{C}^R$ and $\tilde{\epsilon}_{u,t}^{(i)} = \tilde{c}_{u,t}^{(i)} - c_{u,t}$ which denotes the overall error. Then, by (41), the overall error is

$$\tilde{\epsilon}_{u,t}^{(i)} = \underbrace{\left(\sum_{p=1}^{N_{rx}^{RF}} \left[\left(\mathbf{g}_{ad,up,t}^{(i)} \right)^T \bar{\mathbf{H}}_{p,t} \right] - \left(\mathbf{b}_{d,u,t}^{(i)} \right)^T \boldsymbol{\Psi}^{(i-1)} \right) \mathbf{c}_t - c_{u,t}}_{\text{Residual ISI}} - \underbrace{\left(\mathbf{b}_{d,u,t}^{(i)} \right)^T \hat{\epsilon}_t^{(i-1)}}_{\text{Estimate } \hat{\epsilon}_t^{(i)}} + \underbrace{\sum_{p=1}^{N_{rx}^{RF}} \left[\left(\mathbf{g}_{ad,up,t}^{(i)} \right)^T \mathbf{n}_{p,t} \right]}_{\text{Channel Noise}}. \tag{42}$$

As can be observed in (42), the error has three terms:

1. the residual ISI term;
2. the error stemming from the estimate made by $\hat{c}_{u,t}$ of $c_{u,t}$;
3. the term corresponding to the channel noise.

Assuming that the error $\tilde{\epsilon}_{u,t}^{(i)}$ is complex Gaussian distributed then from the Bussgang [70] theorem the zero mean error variable $\hat{\epsilon}_{u,t}^{(i)}$ is uncorrelated with $c_{u,t}$. Therefore, from (42), the average error $\left(\tilde{\epsilon}_{u,t}^{(i)} \right)$ power, i.e., the MSE at time slot t, is given by

$$\begin{aligned} \text{MSE}_{u,t}^{(i)} &= \mathbb{E}[\| \tilde{\epsilon}_{u,t}^{(i)} \|^2] \\ &= \left\| \sum_{p=1}^{N_{rx}^{RF}} \left[\left(\mathbf{g}_{ad,up,t}^{(i)} \right)^T \bar{\mathbf{H}}_{p,t} \right] - \mathbf{v}_u^T - \left(\mathbf{b}_{d,u,t}^{(i)} \right)^T \boldsymbol{\Psi}^{(i-1)} \right\|_F^2 \sigma_u^2 \\ &+ \left\| \left(\mathbf{b}_{d,u,t}^{(i)} \right)^T \left(\mathbf{I}_U - \left| \boldsymbol{\Psi}^{(i-1)} \right|^2 \right)^{1/2} \right\|_F^2 \sigma_u^2 \\ &+ \sum_{p=1}^{N_{rx}^{RF}} \left\| \left(\mathbf{g}_{ad,up,t}^{(i)} \right)^T \right\|_F^2 \sigma_n^2 , \end{aligned} \tag{43}$$

where $\mathbf{v}_u = [0,0,...,1,...,0,0]^T \in \mathbb{C}^U$, with the only non-zero value of $\mathbf{v}_u$ in the *u*th position, and then, $c_{u,t} = \mathbf{v}_u^T \mathbf{c}_t$.

5.2.2 Design of Fully Digital Iterative Multiuser Equalizer

Initially it was considered the optimal case, i.e., a fully digital linear feedforward filter, as shown in Fig. 25, without the sparsity constraint associated with the sub-connected architecture. The design of the iterative multiuser equalizer was based on the IB-DFE principles presented in the chapter 3 and the average BER was used as metric for its design. The average BER minimization, accordingly to [21], is equivalent to the MSE minimization,

$$\begin{aligned}&\left((\mathbf{g}_{ad,up,t}^{(i)})_{opt},(\mathbf{b}_{d,u,t}^{(i)})_{opt}\right)\\&=\arg\min \mathrm{MSE}_{u,t}^{(i)}\\&\text{s.t.}\sum_{t=1}^{T}\sum_{p=1}^{N_{rx}^{RF}}\left(\mathbf{g}_{ad,up,t}^{(i)}\right)^{T}\bar{\mathbf{H}}_{p,t}=T\mathbf{z}_{U}^{T},\end{aligned}\tag{44}$$

where $\mathbf{g}_{ad,up,t}^{(i)}$ is the linear full digital feedforward filter, $\mathbf{b}_{d,u,t}^{(i)}$ the feedback filter and $\mathbf{z}_U=[1,1,...,1]\in\mathbb{C}^U$ a vector with U ones. The solution to the optimization problem (44) by [21] is,

$$\left(\mathbf{g}_{ad,up,t}^{(i)}\right)_{opt}^{T}=\boldsymbol{\omega}_u\left(\bar{\mathbf{H}}_{p,t}\right)^{H}\left(\mathbf{R}_{p,t}^{(i-1)}\right)^{-1}\tag{45}$$

$$(\mathbf{b}_{d,u,t}^{(i)})_{opt}^{T}=\left(\sum_{p=1}^{N_{rx}^{RF}}\left[\left(\mathbf{g}_{ad,up,t}^{(i)}\right)^{T}\bar{\mathbf{H}}_{p,t}\right]-\mathbf{v}_u^{T}\right)\left(\boldsymbol{\Psi}^{(i-1)}\right)^{H},\tag{46}$$

$$\boldsymbol{\omega}_u=T\mathbf{z}_U^{T}\left(\sum_{t=1}^{T}\sum_{p=1}^{N_{rx}^{RF}}\left(\bar{\mathbf{H}}_{p,t}\right)^{H}\left(\mathbf{R}_{p,t}^{(i-1)}\right)^{-1}\bar{\mathbf{H}}_{p,t}\right)^{-1},\tag{47}$$

$$\mathbf{R}_{p,t}^{(i-1)}=\left(\bar{\mathbf{H}}_{p,t}\left(\mathbf{I}_U-\left|\boldsymbol{\Psi}^{(i-1)}\right|\right)\left(\bar{\mathbf{H}}_{p,t}\right)^{H}+\frac{\sigma_n^2}{\sigma_u^2}\mathbf{I}_R\right).\tag{48}$$

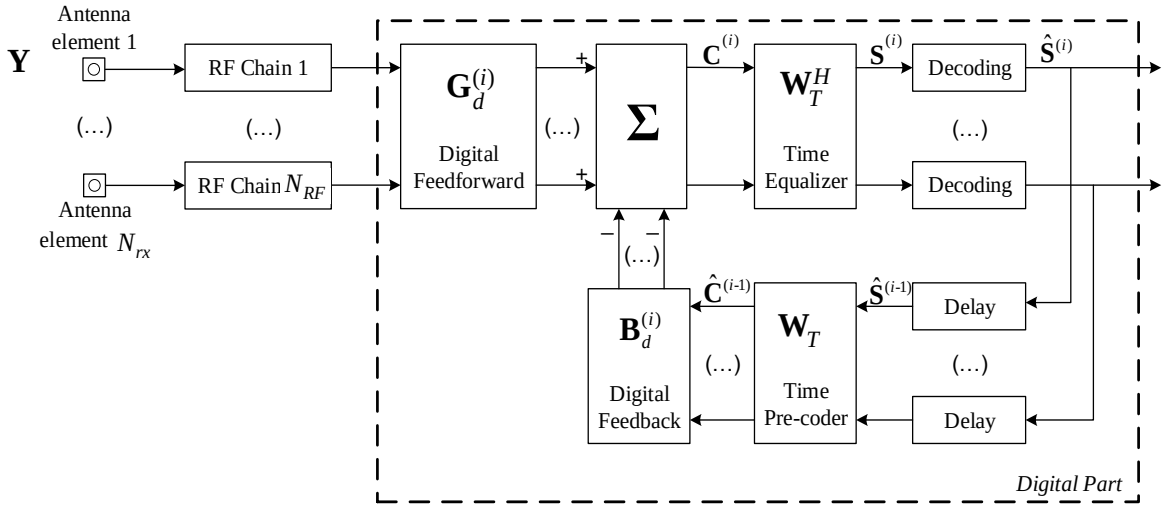

Fig. 25: Full digital Multiuser Equalizer Architecture.

5.2.3 Design of Sub-Connected Hybrid Iterative Multiuser Equalizer

However, the previous optimization problem of (44) does not reflect the analog domain constraints. The set of vectors with constant-magnitude entries, i.e., the set of

feasible RF equalizers was designated as $\mathcal{G}_a$. Thus, the reformulated optimization problem for the sub-connected hybrid iterative equalizer is as follows:

$$\begin{aligned}&\left((\mathbf{g}_{a,u,t}^{(i)})_{opt},(g_{d,up,t}^{(i)})_{opt},(\mathbf{b}_{d,u,t}^{(i)})_{opt}\right)\\&\quad=\arg\min \mathrm{MSE}_{u,t}^{(i)}\\&\qquad\text{s.t.}\sum_{t=1}^{T}\sum_{p=1}^{N_{rx}^{RF}} g_{d,up,t}^{(i)}\left(\mathbf{g}_{a,p,t}^{(i)}\right)^{T}\bar{\mathbf{H}}_{p,t}=T\mathbf{z}_U^{T}\\&\qquad\mathbf{g}_{a,p,t}^{(i)}\in\mathcal{G}_a\ ,\ p\in\left\{1,\ldots,N_{rx}^{RF}\right\}.\end{aligned}\tag{49}$$

The feedback equalizer for the sub-connected hybrid iterative equalizer is analogous to the fully digital iterative equalizer referred to in the previous section, because the analog domain constraints do not impose any restriction on the vector $\mathbf{b}_{d,u,t}^{(i)}$, and thus is given by

$$(\mathbf{b}_{d,u,t}^{(i)})_{opt}^{T}=\left(\sum_{p=1}^{N_{rx}^{RF}}\left[(g_{d,up,t}^{(i)})_{opt}(\mathbf{g}_{a,p,t}^{(i)})_{opt}^{T}\bar{\mathbf{H}}_{p,t}\right]-\mathbf{v}_u^{T}\right)\left(\boldsymbol{\Psi}^{(i-1)}\right)^{H}.\tag{50}$$

According to the constraint of (44) $\sum_{p=1}^{N_{rx}^{RF}}\left[\left(\mathbf{g}_{ad,up,t}^{(i)}\right)_{opt}^{T}\bar{\mathbf{H}}_{p,t}\right]=\mathbf{v}_u^{T}$ and from both (43) and (50), the MSE expression is

$$\begin{aligned}\mathrm{MSE}_{u,t}^{(i)}=&\left\|\sum_{p=1}^{N_{rx}^{RF}}\left[\left(g_{d,up,t}^{(i)}\left(\mathbf{g}_{a,p,t}^{(i)}\right)^{T}-\left(\mathbf{g}_{ad,up,t}^{(i)}\right)_{opt}^{T}\right)\bar{\mathbf{H}}_{p,t}\right]\right.\\&\left.\times\left(\mathbf{I}_U-\left|\boldsymbol{\Psi}^{(i-1)}\right|^{2}\right)^{1/2}\right\|_F^{2}\sigma_u^{2}+\sum_{p=1}^{N_{rx}^{RF}}\left\|g_{d,up,t}^{(i)}\left(\mathbf{g}_{a,p,t}^{(i)}\right)^{T}\right\|_F^{2}\sigma_n^{2}.\end{aligned}\tag{51}$$

Because the feasible set $\mathcal{G}_a$ has a nonconvex nature, an analytical solution to the problem (49) is very hard to obtain. However, an approximate solution is possible by assuming that the vector $\mathbf{g}_{a,p,t}^{(i)}$ is a version of vector $\mathbf{a}_{rx,p}\left(\theta_{j,l}^{rx,p}\right)$. The matrix with the array response vectors of the receiver is formed as $\mathbf{A}_{rx}=\left[\mathbf{A}_{rx,1},\ldots,\mathbf{A}_{rx,U}\right]\in\mathbb{C}^{N_{rx}\times N_{cl}N_{ray}U}$, with $\mathbf{A}_{rx,u}=\left[\mathbf{a}_{rx,u}\left(\theta_{1,1}^{rx,u}\right),\ldots,\mathbf{a}_{rx,u}\left(\theta_{N_{cl},N_{ray}}^{rx,u}\right)\right]\in\mathbb{C}^{N_{rx}\times N_{cl}N_{ray}}$, corresponding to user u. As each RF chain is not connected to all antennas, in the selection process of the vector for the pth RF chain, the entries corresponding to the unconnected antennas are removed. For the uth RF chain is used the dictionary $\mathbf{A}_{rx}^{u}=\left[\mathbf{A}_{rx}(j,l)\right]\in\mathbb{C}^{R\times N_{cl}N_{ray}U}$, where $R(u-1)+1\le j\le Ru$ and

$1 \le l \le N_{cl} N_{ray} U$, which is a sub-matrix of $\mathbf{A}_{rx}$. This approach facilitates the construction of the matrix presented in (35), which corresponds to the statically sub-connected architecture addressed in 4.5. Then, the vector $\mathbf{g}_{a,u,t}^{(i)}$ is selected from dictionary $\mathbf{A}_{rx}^{u}$. Therefore, the optimization problem (49) can be approximated as follows:

$$\begin{aligned} &\left(\ddot{\mathbf{g}}_{d,up,t}^{(i)}\right)_{opt} \\ &= \arg\min \overline{\mathrm{MSE}}_{u,t}^{(i)}\left(\ddot{\mathbf{g}}_{d,up,t}^{(i)}, \mathbf{A}_{rx}^{p}\right) \\ &\quad \mathrm{s.t} \sum_{t=1}^{T}\sum_{p=1}^{N_{rx}^{RF}} \ddot{\mathbf{g}}_{d,up,t}^{(i)}\left(\mathbf{A}_{rx}^{p}\right)^{H} \bar{\mathbf{H}}_{p,t} = T\mathbf{z}_{U}^{T} \\ &\quad \left\| \ddot{\mathbf{g}}_{d,up,t}^{(i)}\left(\ddot{\mathbf{g}}_{d,up,t}^{(i)}\right)^{H} \right\|_{0} = 1, \end{aligned} \tag{52}$$

where $\ddot{\mathbf{g}}_{d,up,t}^{(i)} = \left[g_{d,up,t}^{(i)}, \mathbf{0} \right]^{T} \in \mathbb{C}^{N_{cl}N_{ray}U}$ and

$$\begin{aligned} &\overline{\mathrm{MSE}}_{u,t}^{(i)}\left(\ddot{\mathbf{g}}_{d,up,t}^{(i)}, \mathbf{A}_{rx}^{p}\right) \\ &= \left\| \sum_{p=1}^{N_{rx}^{RF}} \left[\left(\ddot{\mathbf{g}}_{d,up,t}^{(i)}\left(\mathbf{A}_{rx}^{p}\right)^{H} - \left(\mathbf{g}_{ad,up,t}^{(i)}\right)_{opt} \right) \bar{\mathbf{H}}_{p,t} \right] \times \left(\mathbf{I}_{U} - \left| \boldsymbol{\Psi}^{(i-1)} \right|^{2} \right)^{1/2} \right\|_{F}^{2} \sigma_{u}^{2} . \\ &\quad + \sum_{p=1}^{N_{rx}^{RF}} \left\| \ddot{\mathbf{g}}_{d,up,t}^{(i)}\left(\mathbf{A}_{rx}^{p}\right)^{H} \right\|_{F}^{2} \sigma_{n}^{2} \end{aligned} \tag{53}$$

The constraint $\left\| \ddot{\mathbf{g}}_{d,up,t}^{(i)} (\ddot{\mathbf{g}}_{d,up,t}^{(i)})^{H} \right\|_{0} = 1$ enforces that only one element of vector $\ddot{\mathbf{g}}_{d,up,t}^{(i)}$ is non-zero, representing the sparsity constraint. The optimum digital feedforward vector $\left(g_{d,up,t}^{(i)}\right)_{opt}$ is computed from the solution $(\ddot{\mathbf{g}}_{d,up,t}^{(i)})_{opt}$ of the optimization problem in (52), by removing the zero elements. The optimum analog feedforward vector $(\mathbf{g}_{a,u,t}^{(i)})_{opt}$ is given by the selected column from $\left(\mathbf{A}_{rx}^{u}\right)^{H}$, corresponding to the non-zero element of $\ddot{\mathbf{g}}_{d,up,t}^{(i)}$. After obtaining $g_{d,up,t}^{(i)}$, the optimum value of the digital feedforward part, the previous steps are repeated until $u = N_{rx}^{RF}$. All steps are synthesized in *Algorithm 1* where we present the pseudo-code of the proposed sub-connected hybrid iterative block multiuser equalizer.

Algorithm 1: The proposed multiuser Equalizer for sub-connected mmWave massive MIMO architecture

Input: $(\mathbf{g}_{ad,up,t}^{(i)})_{opt}$

1: **for** $u \le N_{rx}^{RF}$ **do**

2:
$$\mathbf{g}_{res,uu,t}^{(i)} = \left(g_{d,uu,t}^{(i)}\mathbf{g}_{a,u,t}^{(i)} - (\mathbf{g}_{ad,uu,t}^{(i)})_{opt}\right)\bar{\mathbf{H}}_{u,t}\left(\mathbf{I}_U - \left|\boldsymbol{\Psi}^{(i-1)}\right|^2\right)\left(\bar{\mathbf{H}}_{u,t}\right)^H + g_{d,uu,t}^{(i)}\mathbf{g}_{a,u,t}^{(i)}\frac{\sigma_n^2}{\sigma_u^2} + \frac{\mu_u}{2\sigma_u^2}\left(\bar{\mathbf{H}}_{u,t}\right)^H$$

3: $k = \arg\max_{l=1,..,N_{cl}N_{ray}}\left((\mathbf{A}_{rx}^{u})^H(\mathbf{g}_{res,uu,t}^{(i)})^H\mathbf{g}_{res,uu,t}^{(i)}(\mathbf{A}_{rx}^{u})\right)_{l,l}$

4: $(\mathbf{g}_{a,u,t}^{(i)})_{opt} = [((\mathbf{g}_{a,u,t}^{(i)})_{opt})^H \mid (\mathbf{A}_{rx}^{u})^{(k)}]^H$

5: **end for**

6: $(g_{d,up,t}^{(i)})_{opt} = \boldsymbol{\omega}_d\left(\bar{\mathbf{H}}_{p,t}\right)^H(\mathbf{g}_{a,p,t}^{(i)})^H\left(\mathbf{g}_{a,p,t}^{(i)}\mathbf{R}_{p,t}^{(i-1)}(\mathbf{g}_{a,p,t}^{(i)})^H\right)^{-1}$

7: **Return** $(\mathbf{g}_{a,u,t}^{(i)})_{opt}$ **,** $(g_{d,up,t}^{(i)})_{opt}$

5.3 Performance Results

The proposed sub-connected hybrid iterative multiuser equalizer is denominated by *"sub-connect"* in the following. The results of the proposed hybrid equalizer are compared against both the fully digital equalizer, denominated by *"digital"*, and fully connected approaches, denoted *"fully connected"*, which was recently proposed in [21]. In this section, it is shown the performance of the proposed hybrid iterative block multiuser equalizer for sub-connected millimeter wave massive MIMO systems. The performance metric considered is the BER, presented as a function of the E_b/N_0, where E_b is the average bit energy and N_0 is the one-sided noise power spectral density. The power of each UT is normalized to $\sigma_1^2 = \ldots = \sigma_U^2 = 1$ and the channel matrix, as previously mentioned, is normalized such that $\mathbb{E}\left[\left\|\mathbf{H}_u\right\|_F^2\right] = N_{rx}N_{tx}$. Therefore, the average E_b/N_0 for all users $u \in \{1,...,U\}$ is identical and given by $E_b/N_0 = \sigma_u^2/\left(2\sigma_n^2\right) = \sigma_n^{-2}/2$. The carrier frequency

was set to 72 GHz and was considered a clustered narrowband channel model [72] for each user with $N_{cl} = 8$ clusters, all with the same average power, and $N_{ray} = 4$ rays per cluster.

The azimuth angles of arrival and departure of the channel model are Laplacian distributed as in [20]. An angle spread equal to 8º degrees, at both the transmitter and receiver, and uniform linear arrays (ULAs) with antenna element spacing equal to half-wavelength were assumed. However, the sub-connected hybrid equalizer developed in this work can be applied to any antenna array configuration. The channel remains constant during a block with size $T = 32$ but varies independently between them. It was assumed perfect synchronization and CSI knowledge at the receiver side. All results were obtained for a QPSK modulation.

At this point, the results are presented for two main scenarios, all with $N_{tx} = 8$. The other parameters were the number of antennas per RF chain, $R = N_{rx} / N_{rx}^{RF}$, and the number of receive antennas, N_{rx}, which are defined for two scenarios as presented in Tab. 2. In both scenarios, the full load case (worst case) is assumed, where the number of users and RF chains is equal. To compute the proposed sub-connected hybrid equalizer it is considered that $\mathbf{f}_{a,u,t}$, the analog precoder for the *u*th user, is generated according to (31). The motivation is to keep the UTs with very low complexity without the knowledge of CSI before transmission. Furthermore, it is important to note that for both scenarios only the static sub-connected approach is considered.

Tab. 2: Parameters for each scenario.

Scenario 1: $U = N_{rx}^{RF} = 8$	Scenario 2: $U = N_{rx}^{RF} = 4$
1.a) $N_{rx} = 16 \ \ (R = 2)$	**2.a)** $N_{rx} = 8 \ \ (R = 2)$
1.b) $N_{rx} = 32 \ \ (R = 4)$	**2.b)** $N_{rx} = 16 \ \ (R = 4)$
1.c) $N_{rx} = 48 \ \ (R = 6)$	**2.c)** $N_{rx} = 24 \ \ (R = 6)$

Initially, the results obtained for scenario 1.b) shown in Fig. 26 and Fig. 27 are presented. In Fig. 26 it is presented results for iteration 1, 2, 3 and 4 of the proposed sub-connected hybrid iterative multiuser equalizer. It can be seen that the performance improves as the number of iterations increases, as expected. Additionally, the gaps between the 1st and 2nd iterations are much higher than between the 3rd and 4th iterations. This occurs

because most of the residual intersymbol and multiuser interferences are removed from the 1st to the 2nd iteration.

Still, for the scenario 1.b), the results with the fully digital and fully connected hybrid multiuser equalizer are presented in Fig. 27. In this figure, it can be seen that the *sub-connect* performance is worse than both *digital* and *fully connect* approaches, mainly for the first iteration. However, for the 4th iteration, it is possible to see that the performance of the proposed sub-connected hybrid multiuser equalizer is close to the *digital* and *fully connect* counterparts. Therefore, it is possible to argue that the dictionary approximation and the sequential optimization are quite precise.

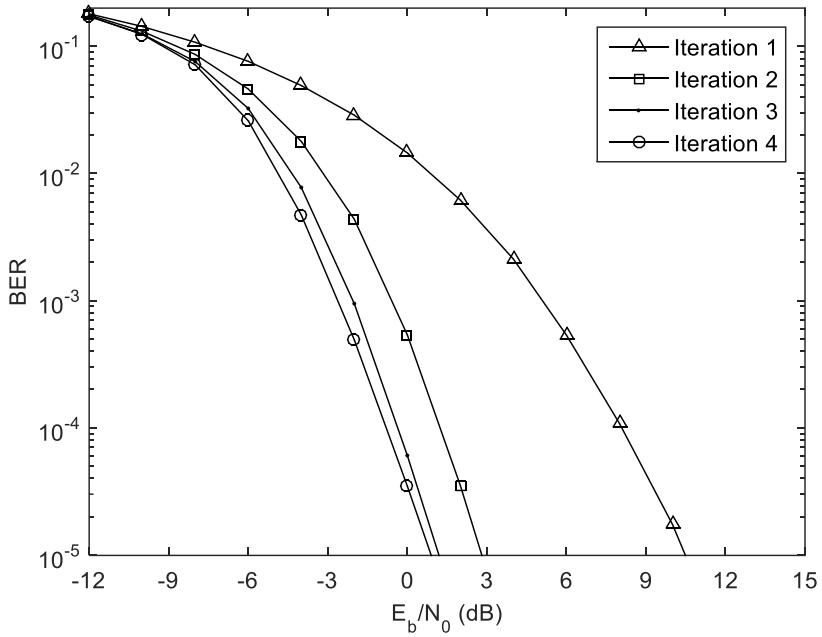

Fig. 26: Performance of the proposed sub-connected hybrid multiuser equalizer for scenario 1.b).

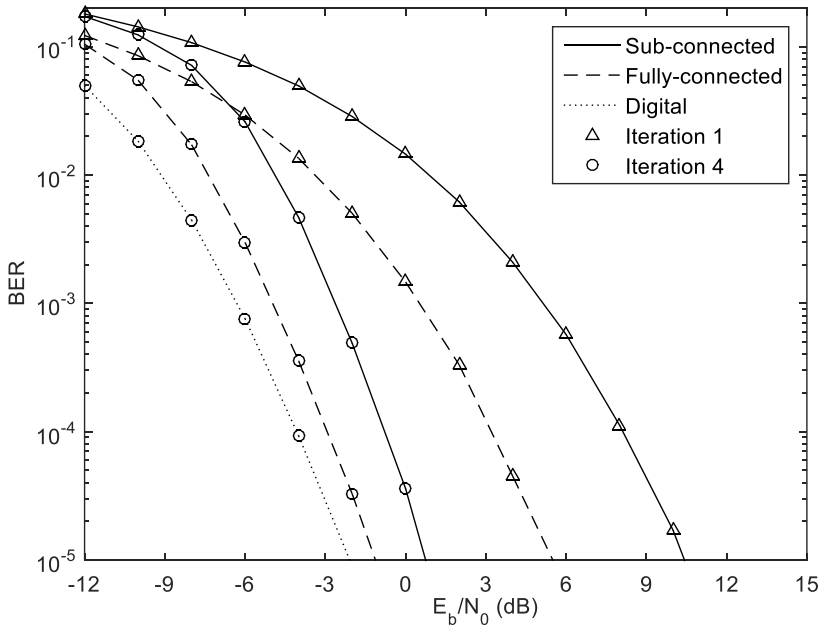

Fig. 27: Performance comparison of the proposed sub-connected hybrid multiuser equalizer with the fully-connected and digital approaches for scenario 1.b).

Comparing the previous scenario 1.b) with scenario 2.b) presented in Fig. 28, where the number of users and RF chains $\left(U = N_{rx}^{RF}\right)$ changes, but the number of antennas per RF chain is the same, i.e., $R = 4$. In scenario 1.b, at a target BER of 10^{-3} and iteration 4, the penalties of the proposed sub-connected equalizer for *fully connect* and *digital* approaches are 2.3 dB and 3.8 dB. In scenario 2.b, for the same target BER and iteration, the penalties for *fully connect* and *digital* are approximately 1.6 dB and 3.2 dB, slightly decreasing for lower $U = N_{rx}^{RF}$. It can also be seen that for scenario 1.b) a lower E_b/N_0 is needed to achieve a BER of 10^{-5} compared with scenario 2.b). This is because scenario 1.b) can achieve higher diversity and array gain given by the larger dimension of the receiving antenna array.

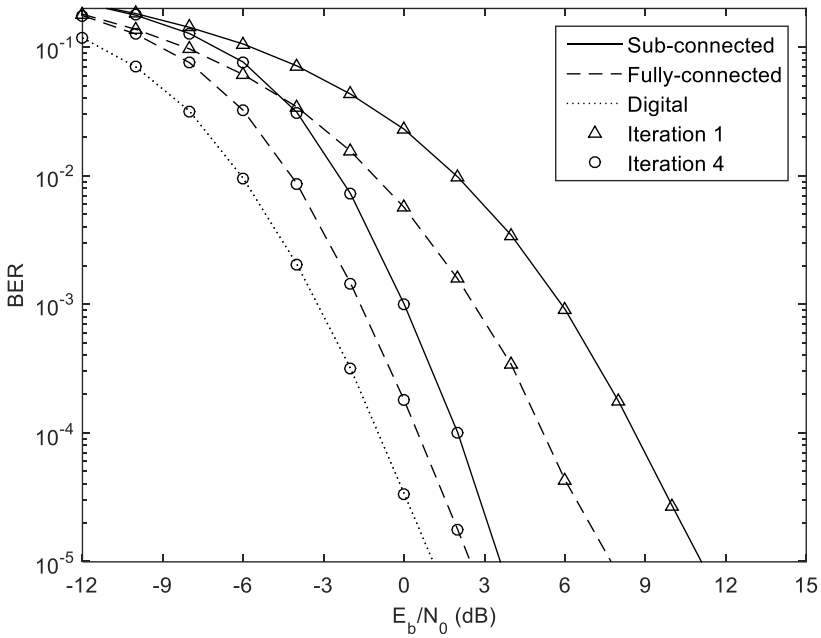

Fig. 28: Performance comparison of the proposed sub-connected hybrid multiuser equalizer with the fully-connected and digital approaches for scenario 2.b).

When the number of antennas per RF chain is reduced by half, i.e., for $R=2$, which corresponds to scenario 1.a) presented in Fig. 29, it turns out that the penalty for *fully connected* and *digital* approaches is approximately 1.2 dB and 1.9 dB, thus decreasing for lower R.

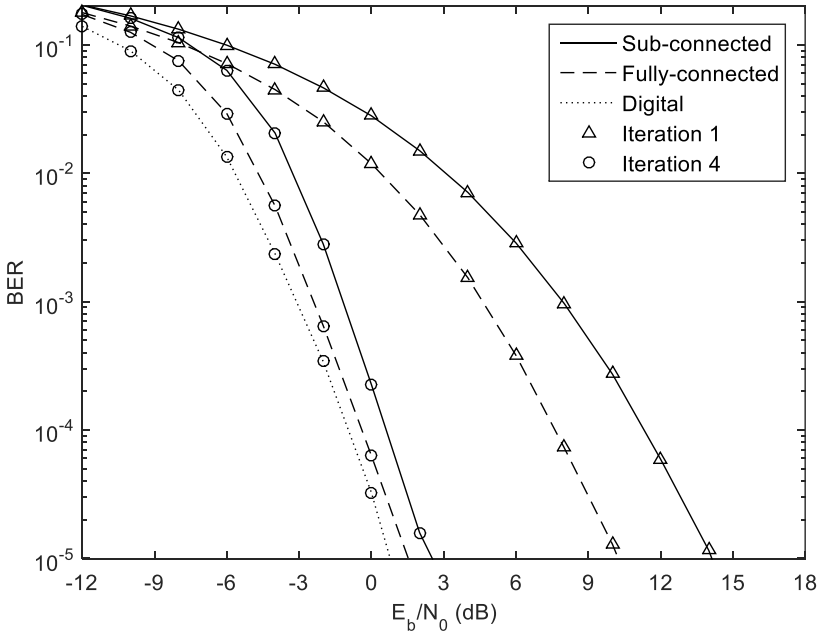

Fig. 29: Performance comparison of the proposed sub-connected hybrid multiuser equalizer the fully-connected and digital approaches for scenario 1.a).

This occurs because when R is reduced, the sub-connected architecture tends toward the fully digital case. In the extreme case where $R=1$, only one antenna is connected to one RF chain i.e., the digital architecture. As expected, by reducing R the degrees of freedom of the sub-connected architecture increase, and the gap with the *fully connected* and *digital* approaches decreases.

In Fig. 30 and Fig. 31, we compare the performance of the *sub-connect* approach for scenario 1 and 2 by considering $R=2,\ 4$ and 6 antennas per RF chain. As previously verified, the penalty of the proposed sub-connected multiuser equalizer relative to the *fully connected* and *digital* increases with R. Nevertheless, the BER performance of the sub-connected multiuser equalizer improves with R, because the diversity and antenna gains are higher due to a larger number of receiving antennas.

Notably, the above it is considered the worst case, where $U = N_{rx}^{RF}$. For $U < N_{rx}^{RF}$, i.e., for a number of users (streams) lower than the number of RF chains, the BER performance would be improved. For that case, the performance gaps between the proposed sub-connect hybrid multiuser equalizer and the *digital*/*fully connect* approaches would be even smaller.

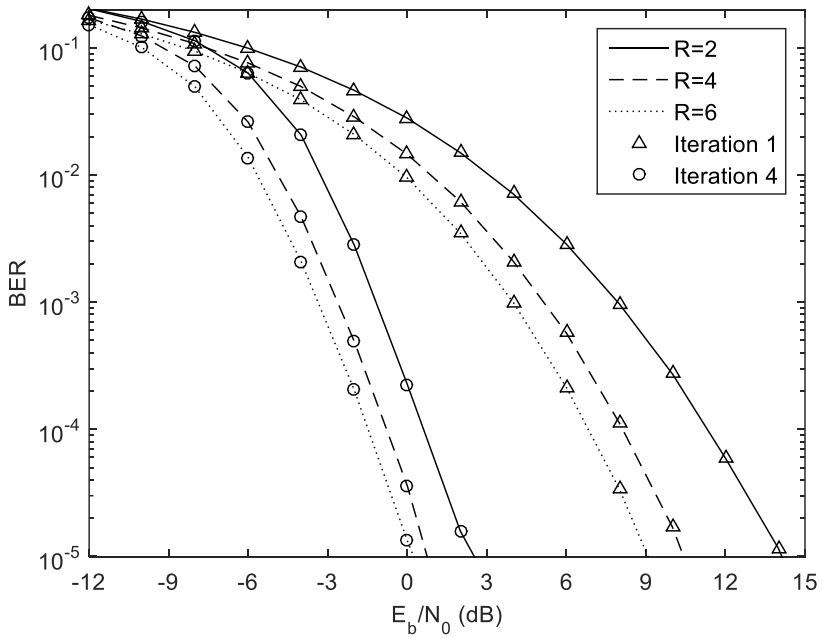

Fig. 30: Performance comparison of the proposed sub-connected hybrid multiuser equalizer for *R*=2, 4 and 6, for scenario 1.

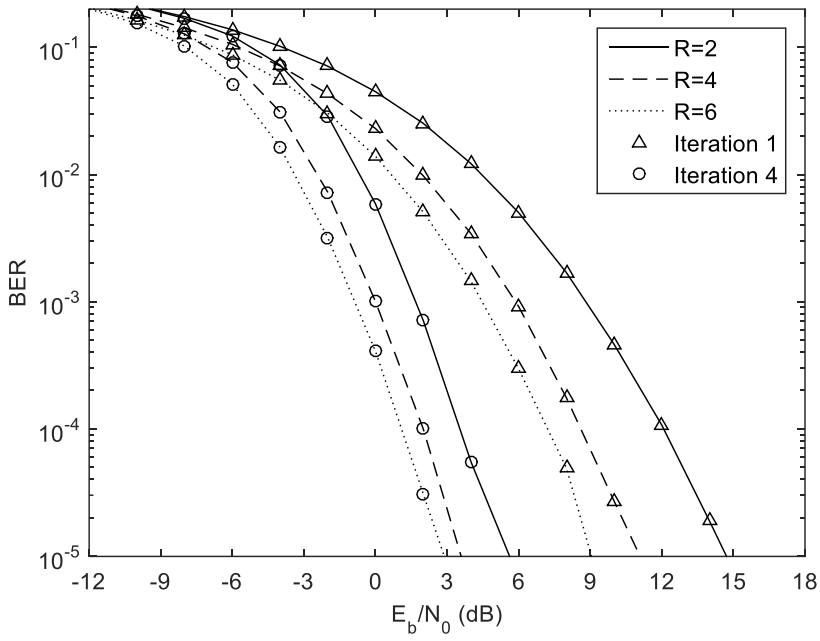

Fig. 31: Performance comparison of the proposed sub-connected hybrid multiuser equalizer for R=2, 4 and 6, for scenario 2.

In Fig. 32 and Fig. 33 it is presented results for different number of users when compared to what was presented previously, but maintaining the number of RF chains equal to $N_{rx}^{RF} = 8$.

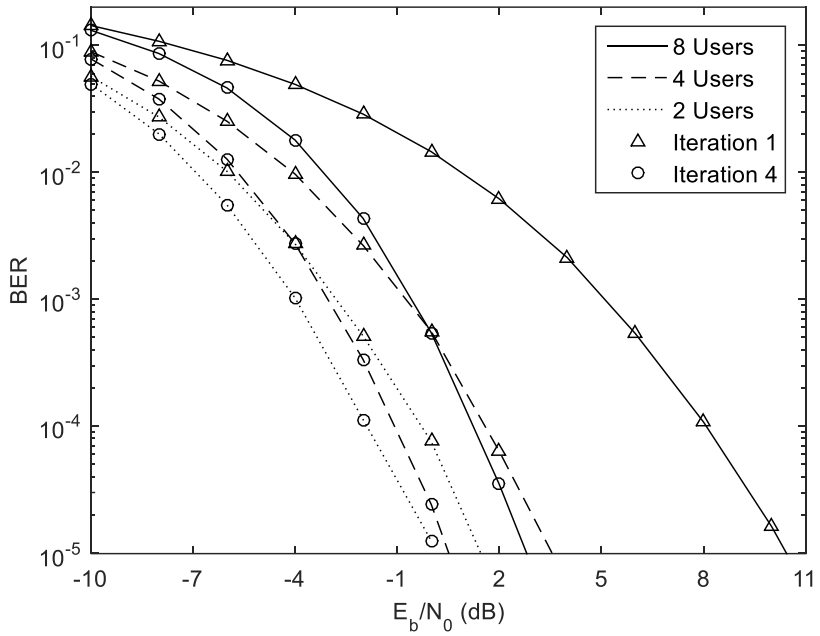

Fig. 32: Performance comparison of the proposed sub-connected hybrid multiuser equalizer for $U = 8$, 4 and 2, $N_{tx} = 8$, $N_{rx}^{RF} = 8$ and $R = 4$.

Fig. 32 shows the BER performance for the proposed sub-connected hybrid iterative multiuser equalizer, when the number of users decreases from 8 to 2 and the number of RF chains remain constant $\left(N_{rx}^{RF}=8\right)$. As excpected the BER performance improves when the number of users decreases, for both iterations 1 and 4. The Fig. 33 allows to compare the *sub-connect* approach with the *fully connected* and *digital*, when the number of users is less than the number of RF chains. In this case we have $U=4$, where each user u has $N_{tx}=8$ and $N_{rx}^{RF}=4$. At this point we can compare the Fig. 28 (scenario 2.b)) and Fig. 33, because the only difference between them is that the number of users was reduced for the results presented in this Fig. 33. Thus, analysing both figures we can see that the gap between *fully connected* and *sub-connect* decreases by 1.5 dB, for the first iteration. The gap between *digital* and *sub-connect* decrease by 0.53 dB, for the fourth iteration. Thus, with a lower of the number of users the BER performance improves as expected.

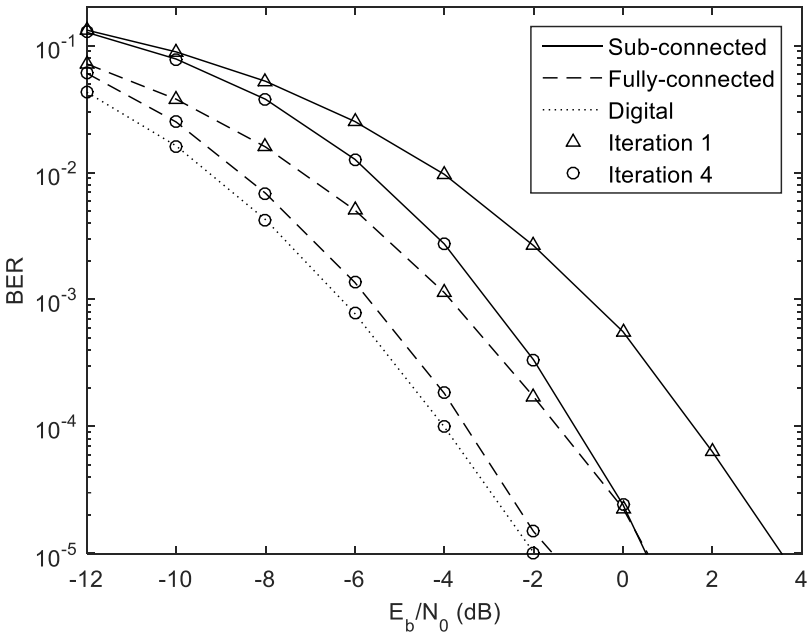

Fig. 33: Performance comparison of the proposed sub-connected hybrid multiuser equalizer for $U=4$, $N_{tx}=8$, $N_{rx}^{RF}=4$ and $R=4$.

6 Conclusions and Future Work

From analog to LTE, all improvements in mobile systems were driven by the need to meet ever more demanding requirements. To achieve the new requirements, the 5G will need a paradigm shift that includes very high carrier frequencies with massive bandwidths, very high density and coverage and an unprecedented number of antennas. As discussed in this dissertation, two enabling technologies have been considered to meet the QoS requirements for future 5G wireless communication, and they are the mMIMO and mmWave communications. With mmWave and mMIMO combination we can exploit new efficient spatial processing techniques, such as beamforming and spatial multiplexing, at the transmitter and receiver sides. However, these new technologies imply certain limitations and hardware constraints. The aim of this work is to present a feasible solution for a hardware structure that uses the presented new technologies to reach the QoS requirements for the new mobile generation.

6.1 Conclusions

This dissertation started by presenting an overview of the evolution of mobile communications which culminated in the 5G, the next generation of telecommunication systems. A brief discussion about the direction of the evolution and some key requirements was also provided. In the first chapter, it was presented the state of the art, where it was discussed theoretically the essential concepts required for the development of this work.

The second chapter, first describes the multiple antenna systems and presents some of its weaknesses and respective possible solutions. At the end of this chapter the mMIMO concept is introduced, always focusing on the requirements needed to reach the fifth generation of mobile communication systems.

In the third chapter we describe digital techniques of equalization, for both the linear and nonlinear/iterative based equalizers.

The fourth chapter addressed the mmWave communication technology, jointly with some of its specific aspects such as the spectrum and attenuation bands. As the mmWave mMIMO combination represents an approach to achieve the multigigabit data rates and other QoS requirements this chapter introduces the hybrid architectures that allows to blend both technologies.

In the fifth chapter, a new hybrid iterative multiuser equalizer for a mmWave mMIMO system with sub-connected architecture and low-complexity UTs was designed. As the transition from digital to hybrid architectures is an important aspect of this work, the iterative receiver is described for both. The fifth chapter also presents the results obtained during this thesis, which include the simulations of the hybrid iterative multiuser equalizer for a sub-connected mmWave massive MIMO architecture. From these results, it was observed that by reducing the number of receiving antennas per RF chain, i.e., $R = N_{rx} / N_{rx}^{RF}$, the BER performance gets worse. That is explained by the reduction of both the antenna gain and diversity. It was also observed that the gap between the proposed *sub-connect* scheme and the *digital*/*fully connect* approaches decreases when R decreases, because the architecture becomes closer to the *digital* one.

The proposed objectives were met, since at the end of this dissertation, a sub-connected hybrid architecture was designed for mmWave mMIMO systems and the performance of the projected receiver structure shows that it is interesting for practical mmWave mMIMO based systems. It has been proven that for systems with hardware constraints the number of transmit/receive RF chains can be much lower than the number of transmit/receive antennas, and each RF chain can be only connected to a reduced number of antennas, ensuring good performance at a low cost. Some specific conclusions can be pointed out:

- The proposed iterative equalizer needs just a few iterations to reach significant improvements in the BER performance. This is verified because most of the residual intersymbol and multiuser interferences are removed from the 1st to the 2nd iteration;
- Increasing the number of antennas per RF chain the BER, of the proposed sub-connected hybrid iterative multiuser equalizer, decreases. This occurs

due to the fact that if we increase the number of antennas then the diversity and array gain also increase;

- If the number of antennas at the BS is kept fixed but the number of RF chains increases, which means less antennas per RF chain, the BER performance gap between the proposed sub-connected hybrid iterative multiuser equalizer and the *fully connected* and *digital* approaches decreases. By reducing the number of antennas per RF chain, the degrees of freedom of the sub-connected architecture increase and the gap between the *fully connected* and *digital* approaches decreases, until we get to the case where we have only one antenna per RF chain, i.e., the digital case.
- The BER performance improves with the decrease of the number of users. This behavior is explained because the interuser interferece and intersymbol interference decrease.

6.2 Future Work

To finish this dissertation some suggestions for future work is presented. In this work, some assumptions were made regarding the system under consideration. Namely, it was assumed a system with perfect synchronization and CSI knowledge at the receiver side. The way to test this system in other environments would be to observe how the proposed system would behave with imperfect channel information or with synchronisation errors. In the proposed sub-connected hybrid iterative multiuser equalizer, at the analog part, the connection between each RF chain is performed statically. It would be interesting to evaluate the performance of a sub-connected hybrid iterative multiuser equalizer where the connection between each RF chain and a subset of antennas is done dynamically.

On the other hand, at the UTs with the conjugation of the mmWave and mMIMO technologies it is possible to pack a very large number of antennas in a small area, therefore the number of antennas in each UT can be increased. The higher number of antennas at the UTs enable different options for the architecture and system configuration. Namely, a possible future work could be to design a user terminal with more than one RF chain, sending more than one data stream per time slot. Two other interesting cases for study in future works would be to design a sub-connected hybrid architecture for the UTs, with a static connection

between each RF chain and a set of antennas or with dynamically connection, where each RF chain can dynamically connect to a different set of antennas.

7 References

[1] About 3GPP, “The MobileBroadband Standard”, [Available Online] http://www.3gpp.org/about-3gpp.

[2] M. Jaloun, Z. Guennoun, “Wireless Mobile Evolution to 4G Network”, *Wireless Sensor Network*, 2010, 2, 309-317.

[3] T. S. Rappaport, S. Sun, R. Mayzus, H. Zhao, Y. Azar, K. Wang. G. N. Wong, J. K. Schulz, M. Samimi and F. Gutierrez, “Millimeter Wave Mobile Communications for 5G Cellular: It Will Work”, in *IEEE Access*, vol. 1, no. , pp. 335-349, 2013.

[4] Ericsson, "Ericsson Mobility Report", Executive Report from Ericsson, Huawei and Qualcomm, June 2017, [Available Online] https://www.ericsson.com/assets/local/mobility-report/documents/2017/ericsson-mobility-report-june-2017.pdf.

[5] SK Telecom, “SK telecom 5G white paper”, October 2014, [Available Online] http://www.sktelecom.com/img/pds/press/SKT_5G%20White%20Paper_V1.0_Eng.pdf.

[6] Global mobile Suppliers Association, "The Road to 5G: Drivers, Applications, Requirements and Technical Development", Executive Report from Ericsson, Huawei and Qualcomm, November 2015.

[7] J. G. Andrews *et al*., "What Will 5G Be?", in *IEEE Journal on Selected Areas in Communications*, vol. 32, no. 6, pp. 1065-1082, June 2014.

[8] A. L. Swindlehurst, E. Ayanoglu, P. Heydari and F. Capolino, "Millimeter-wave massive MIMO: the next wireless revolution?", in *IEEE Communications Magazine*, vol. 52, no. 9, pp. 56-62, September 2014.

[9] K. Zheng, L. Zhao, J. Mei, B. Shao, W. Xiang and L. Hanzo, "Survey of Large-Scale MIMO Systems", in *IEEE Communications Surveys & Tutorials*, vol. 17, no. 3, pp. 1738-1760, thirdquarter 2015.

[10] C. Dehos, J. L. González, A. De Domenico, D. Kténas, and L. Dussopt, “Millimeter-wave access and backhauling: the solution to the exponential data traffic increase in 5G mobile communications systems?”, *IEEE Communications Magazine*, vol. 52, no. 9, Sept. 2014, pp.88-95.

[11] L. van der Perre, S. Pollin, W. Dehaene, E. G. Larsson, E. Björnson, O. Edfors, L. Liu, F. Tufvesson, A. Bourdoux, C. Desset, F. Dielacher, J. Lorca Hernando, K. M. Koch, T. L. Marzetta, P. Demeester, J. Rabaey, A. Gatherer, "Resurrection of 5G: In defense of Massive MIMO", *IEEE ComSoc Technology News*, 2016.

[12] T. Baykas, Chin-Sean Sum, Z. Lan, J. Wang, M. A. Rahman and H. Harada, NICT Shuzo, NICT and Tohoku University, "IEEE 802.15.3c: the first IEEE wireless standard for data rates over 1 Gb/s", in *IEEE Communications Magazine*, vol. 49, no. 7, pp. 114-121, July 2011.

[13] A. Akhtar and S. C. Ergen, "Efficient network level beamforming training for IEEE 802.11ad WLANs", *2015 International Symposium on Performance Evaluation of Computer and Telecommunication Systems (SPECTS)*, Chicago, IL, 2015, pp. 1-6.

[14] A. Gupta, R. K. Jha, "A Survey of 5G Network: Architecture and Emerging Technologies", *IEEE Access*, vol.3, pp. 1206-1232, July 2015.

[15] W. Roh, *et all.*, "Millimeter-wave beamforming as an enabling technology for 5G cellular communications: theoretical feasibility and prototype results", in *IEEE Communications Magazine*, vol. 52, no. 2, pp. 106-113, February 2014.

[16] O. E. Ayach, S. Rajagopal, S. Abu-Surra, Z. Pi and R. W. Heath, "Spatially Sparse Precoding in Millimeter Wave MIMO Systems", in *IEEE Transactions on Wireless Communications*, vol. 13, no. 3, pp. 1499-1513, March 2014.

[17] X. Gao, L. Dai, C. Yuen, and Z. Wang, “Turbo-like beamforming based on Tabu search algorithm for millimeter-wave massive MIMO systems”, IEEE *Trans. Veh. Technol.*, vol. 65, no. 7, pp. 5731-5737, Jul. 2015.

[18] Z. Xiao, T. He, P. Xia, and X.-G. Xia, “Hierarchical codebook design for beamforming training in millimeter-wave communication”, IEEE *Trans. Wireless Commun.*, vol. 15, no. 5, pp. 3380-3392, May 2016.

[19] J. Li, L. Xiao, X. Xu, and S. Zhou, “Robust and low complexity hybrid beamforming for uplink multiuser mmWave MIMO systems”, IEEE *Commun. Letters*, vol. 20, no. 6, Jun. 2016.

[20] A. Alkhateeb, G. Leus, and R. Heath, Jr., “Limited feedback hybrid precoding for multi-user millimeter wave systems”, *IEEE Trans. Wireless Commun.*, vol. 14, no. 11, pp. 6481–6404, Nov. 2015.

[21] R. Magueta, D. Castanheira, A. Silva, R. Dinis, and A. Gameiro, “Hybrid Iterative Space-Time Equalization for Multi-User mmW Massive MIMO Systems”, IEEE *Trans. on Commun.*, vol.65, no. 2, pp. 608-620, Feb. 2017.

[22] S. Mumtaz, J. Rodriguez, and L. Dai, “mmWave Massive MIMO: A Paradigm for 5G”, *Academic Press*, 1st Edition, Nov. 2016.

[23] Islam J. (2012), **“**Performance Analysis of Diversity Techniques for Wireless Communication System, Blekinge Institute of Technology”, Master's thesis in Electrical Engineering emphasis on Telecommunication, pp. 74, Feb. 2012.

[24] David Gozálvez Serrano, “Combined Time, Frequency and Space Diversity in Multimedia Mobile Broadcasting Systems”, Departamento de Comunicaciones, Universitat Politècnica de València, PhD final thesis, pp. 173, 2012.

[25] M. Makni, J. Robert and E. Stare, "Performance analysis of time frequency slicing", *2011 14th ITG Conference on Electronic Media Technology*, Dortmund, 2011, pp. 1-6.

[26] Y. Huang and K. Boyle, Antennas From Theory to Practice, Chichester: A John Wiley and Sons Ltd, 2008.

[27] Andreas F. Molisch, *Wireless Comunications*, John Wiley & Sons Ltd. 2011.

[28] A. Silva and A. Gameiro "Multiple Antenna Systems", University of Aveiro: Comunicações Sem Fios Lecture, 2015/16.

[29] Raqibul Mostafa, Ramesh C. Pallat, Uwe Ringel, Ashok A. Tikku, and Je_rey H. Reed, "Closed-Loop Transmit Diversity Techniques for Small Wireless Terminals and Their Performance Assessment in a Flat Fading Channel", *ETRI Journal*, vol. 34, no. 3, June 2012.

[30] Siavash M. Alamouti "A Simple Transmit Diversity Technique for Wireless Communications", *IEEE Journal* on select areas in communications, vol. 16, no. 8, pp. 1451-1458, October 1998.

[31] Tarokh, H. Jafarkhani, A.R. Calderbank, ”Space-time block coding for wireless communications: Performance results”, IEEE Journal on Sel. Areas in Com., vol.17, no. 3, pp. 451-460, Mar. 1999.

[32] B. Badic, M. Rupp and H. Weinrichter, "Quasi-Orthogonal Space-Time Block Codes: Approaching optimality", *2005 13th European Signal Processing Conference*, Antalya, 2005, pp. 1-8.

[33] G. Jongren and S. Sorrentino, *Spatial multiplexing communication system with enhanced code-word mapping with flexible rate selection on each spatial layer and with single harq process*, May 13 2014, US Patent 8,726,131.

[34] Jan Mietzner, “Spatial Diversity in MIMO Communication Systems with Distributed or Co-located Antennas”, Faculty of Engineering, Christian-Albrechts University of Kiel (CAU), Germany, PhD final thesis, pp. 351, 2007.

[35] B. D. Van Veen and K. M. Buckley, "Beamforming: a versatile approach to spatial filtering", in *IEEE ASSP Magazine*, vol. 5, no. 2, pp. 4-24, April 1988.

[36] Luis García Ordóñez, “Performance Limits of Spatial Multiplexing MIMO Systems, Departement de Teoria del Senyal I Comunicaciones”, Universitat Politècnica de Catalunya, PhD final thesis, pp. 228, March 2009.

[37] Huy Hoang Pham, "A Study on MIMO Beamforming for Wireless Communication Systems in Frequency-Selective Fading channels", University of Electro-Communications, Master's thesis, March 2006.

[38] R. Gaoka and Dr. A. Cheeran, "Performance Analysis of Beamforming Algorithms", *International Journal of Electronics & Communication Technology*, Vol. 2, Issue 1, pp. 2230-9543, March 2011.

[39] Maharimi, S. F., Malek, M. A., Jamlos, M. F., Neoh, S. C., & Jusoh, M. (2012, March). Impact of spacing and number of elements on array factor. In *Proc. of Progress in Electromagnetics ResearchSymposium* (pp. 1550-1553).

[40] X. Chen, J. Lu, T. Li, P. Fan and K. B. Letaief, "Directivity-Beamwidth Tradeoff of Massive MIMO Uplink Beamforming for High Speed Train Communication", in *IEEE Access*, vol. 5, pp. 5936-5946, 2017.

[41] N. Benvenuto, R. Dinis, D. Falconer, and S. Tomasin, "Single carrier modulation with non linear frequency domain equalization: An idea whose time has come - Again", *Proceedings of the IEEE*, vol. 98, no. 1, pp. 69-96, Jan. 2010.

[42] Paliwal, Seema, Dilpreet Kaur Grover, and Jyoti Krayla. "Comparison of Linear and Non-Linear Equalizer using the Maltlab", *Communications on Applied Electronics*, vo. 4, no.1, Jan. 2016.

[43] Y. Jiang, M. K. Varanasi and J. Li, "Performance Analysis of ZF and MMSE Equalizers for MIMO Systems: An In-Depth Study of the High SNR Regime", in *IEEE Transactions on Information Theory*, vol. 57, no. 4, pp. 2008-2026, April 2011.

[44] Conillera Vilar, F. (2015), "Implementation of Zero Forcing and MMSE equalization techniques in OFDM", [Available online] http://hdl.handle.net/2117/78037.

[45] N. Benvenuto, and S. Tomasin, "Block iterative DFE for single carrier modulation", Electron. Lett., vol. 39, no. 19, pp.1144-1145, Sep. 2002.

[46] Y.-C. Liang, S. Sun, and C. K. Ho, "Block-iterative generalized decision feedback equalizers for large MIMO systems: Algorithm design and asymptotic performance analysis", *IEEE Trans. Signal Process.*, vol. 54, no. 6, pp. 2035–2048, June 2006.

[47] R. Kalbasi, D. Falconer, A. Banihashemi and R. Dinis, "A comparison of frequency domain block MIMO transmission systems," *IEEE Trans. Veh. Technol.*, vol. 58, no. 1, pp. 165-175, Jan. 2009.

[48] J. Luzio, R. Dinis, and P. Montezuma, "SC-FDE for offset modulations: An efficient transmission technique for broadband wireless systems", *IEEE Trans. Commun.* vol. 60, no.7, pp. 1851-1861, Jul. 2012.

[49] P. Li and R. C. de Lamare, "Adaptive decision-feedback detection with constellation constraints for MIMO systems", *IEEE Trans. Veh. Technol.*, vol. 61, no. 2, pp. 853–859, Feb. 2012.

[50] A. Silva, T. Teodoro, R. Dinis, and A. Gameiro, "Iterative frequency-domain detection for IA-precoded MC-CDMA systems ", *IEEE Trans. Commun.* vol. 62, no. 4, pp. 1240-1248, April, 2014.

[51] D. Castanheira, A. Silva, R. Dinis, and A. Gameiro, "Efficient transmitter and receiver designs for SC-FDMA based heterogeneous networks", *IEEE Trans. Commun.* vol. 63, no. 7, pp. 2500 - 2510, 2015.

[52] Gant João, "IB-DFE Techniques Apllied to Multi-Antenna Systems", Universidade de Coimbra, Master Thesis in Electrotechnical and Computer Engineering, pp. 71, 2014.

[53] A. Silva, J. Assunção, R. Dinis, A. Gameiro, Performance evaluation of IB-DFE-based strategies for SC-FDMA systems, *EURASIP Journal on Wireless Communications and Networking*, Vol. 2013, No. 1, pp. 1 - 10, December, 2013.

[54] T. Nitsche, C. Cordeiro, A. B. Flores, E. W. Knightly, E. Perahia and J. C. Widmer, "IEEE 802.11ad: directional 60 GHz communication for multi-Gigabit-per-second Wi-Fi [Invited Paper]", in *IEEE Communications Magazine*, vol. 52, no. 12, pp. 132-141, December 2014.

[55] Z. Pi and F. Khan, "An introduction to millimeter-wave mobile broadband systems", in *IEEE Communications Magazine*, vol. 49, no. 6, pp. 101-107, June 2011.

[56] M. Marcus and B. Pattan, "Millimeter wave propagation; spectrum management implications", in *IEEE Microwave Magazine*, vol. 6, no. 2, pp. 54-62, June 2005.

[57] T. E. Bogale and L. B. Le, "Beamforming for multiuser massive MIMO systems: Digital versus hybrid analog-digital", *in Proc. IEEE Global Telecommunication Conf.*, Austin, TX, Dec. 2014, pp. 10–12.

[58] K. Prasad, E.Hossain, V. Bhargava, "Energy Efficiency in Massive MIMO-Based 5G Networks: Opportunities and Challenges", *IEEE Wireless Commun.*, vol. PP, no. 99, pp. 2–10, Jan. 2017.

[59] M. Agiwal, A. Roy, and N. Saxena, "Next Generation 5G Wireless Networks: A Comprehensive Survey", *IEEE Commun. Surveys & Tutorials*, vol. 18, no. 3, pp. 1617-1655, Feb. 2016.

[60] F. Boccardi, R. W. Heath, Jr., A. Lozano, T. L. Marzetta, and P. Popovski, “Five disruptive technology directions for 5G”, *IEEE Commun.* Mag., vol. 52, no. 2, pp. 74–80, Fev. 2014.

[61] L. Lu, G. Li, A. Swindlehurst, A. Ashikhmin, and R. Zhang, “An overview of massive MIMO: Benefits and challenges”, IEEE J. Sel. Topics Signal Process., vol. 8, no. 5, pp. 742–758, Oct. 2014.

[62] T. E. Bogale, L. B. Le, A. Haghighat, and L. Vandendorpe, “On the number of RF chains and phase shifters, and scheduling design with hybrid analog-digital beamforming”, *IEEE Trans. Wireless Commun*., vol. 15, no. 5, pp. 3311-3326, Jan. 2016.

[63] J. Wang et. al., ”Beam codebook based beamforming protocol for multi-Gbps millimeter-wave WPAN systems”, *IEEE J. Sel. Areas Commun.* vol. 27, no. 8, pp. 1390-1399, 2009.

[64] O. El Ayach, R. W. Heath, Jr., S. Abu-Surra, S. Rajagopal, and Z. Pi, “The capacity optimally of beam steering in large millimeter wave MIMO systems”, *in Proc. IEEE International Workshop Signal Process. Advances Wireless Commun.* 2012.

[65] A. Alkhateeb, J. Mo, N. Gonzáles-Prelcic, and R. W. Heath, Jr., “MIMO precoding and combining solutions for millimeter-wave systems”, *IEEE Commun. Mag.*, vol. 52, no. 12, pp. 122–131, 2014.

[66] S. Han, Chih-Li I, Z. Xu, andC. Rowell, “Large-scale antenna systems with hybrid analog and digital beamforming for millimeter wave 5G”, *IEEE Commun. Mag.*, vol. 53, no. 1, pp. 186–194, 2015.

[67] X. Gao, L. Dai, S. Han, Chih-Lin I, R. W. Heath, “Energy-Efficient Hybrid Analog and Digital Precoding for MmWave MIMO Systems With Large Antenna Arrays”, *IEEE Journal on Selected Areas in Commun*., vol. 34, no. 4, pp. 998-1009, April 2016.

[68] S. Park, A. Alkhateeb, and R. W. Heath Jr., “Dynamic subarray architecture for wideband hybrid precoding in millimeterwave MIMO systems”, *IEEE Global Conference on Signal and Information Processing (GlobalSIP)*, vol. 2016, pp. 1-1, Dec. 2016.

[69] S. He, C. Qi, Y. Wu, and Y. Huang, “Energy-Efficient Transceiver Design for Hybrid Sub-Array Architecture MIMO Systems”, *IEEE Access*, vol. 4, pp. 9895-9905, 2016.

[70] H. E. Rowe, “Memoryless nonlinearities with Gaussian inputs: elementary results”, *Bell Syst. Tech. J.*, vol. 61, no. 7, pp.1519-1525, 1982.

[71] R. Magueta, V. Mendes, D. Castanheira, A. Silva, Atilio Gameiro, R. Dinis and, “Iterative Multiuser Equalization for Sub-Connected Hybrid mmWave Massive MIMO Architecture”, submitted to: *Mobile Information Systems*, pp. 11, 2017.

[72] M. R. Akdeniz, Y. Liu, M. K. Samimi, S. Sun, S. Rangan, T. S. Rappaport, and E. Erkip, “Millimeter wave channel modeling and cellular capacity evaluation”, IEEE J. Sel. Areas Commun. vol 32, no. 6, pp. 1164 – 1179, 2014.